



LAWRENCE
LIVERMORE
NATIONAL
LABORATORY

Electronic Structure Differences Between H₂-, Fe-, Co-, and Cu-Phthalocyanine Highly Oriented Thin Films Observed Using NEXAFS Spectroscopy

T. M. Willey, M. Bagge-Hansen, J. R. I. Lee, R. Call, L. Landt, T. van Buuren, C. Colesniuc, C. M. Monton, I. Schuller

October 30, 2012

Journal of Chemical Physics

Disclaimer

This document was prepared as an account of work sponsored by an agency of the United States government. Neither the United States government nor Lawrence Livermore National Security, LLC, nor any of their employees makes any warranty, expressed or implied, or assumes any legal liability or responsibility for the accuracy, completeness, or usefulness of any information, apparatus, product, or process disclosed, or represents that its use would not infringe privately owned rights. Reference herein to any specific commercial product, process, or service by trade name, trademark, manufacturer, or otherwise does not necessarily constitute or imply its endorsement, recommendation, or favoring by the United States government or Lawrence Livermore National Security, LLC. The views and opinions of authors expressed herein do not necessarily state or reflect those of the United States government or Lawrence Livermore National Security, LLC, and shall not be used for advertising or product endorsement purposes.

Electronic Structure Differences Between H₂-, Fe-, Co-, and Cu-Phthalocyanine Highly Oriented Thin Films Observed Using NEXAFS Spectroscopy

T. M. Willey^{1*}, M. Bagge-Hansen¹, J. R. I. Lee¹, R. Call^{1,2}, L. Landt^{1,3}, T. van Buuren¹, C. Colesniuc⁴, C. Monton⁴, I. Valmianski⁴, I. K. Schuller⁴

(1) *Condensed Matter and Materials Division, Lawrence Livermore National Laboratory, CA, USA*

(2) *Department of Physics and Astronomy, Utah State University, Logan, UT, USA*

(3) *Institute for Optics and Atomic Physics, Technischen Universität Berlin, Berlin, Germany*

(4) *Department of Physics, University of California, San Diego, La Jolla, CA, USA*

* *corresponding author*

Phthalocyanines, a class of macrocyclic, square planar molecules, are extensively studied as semiconductor materials for chemical sensors, dye-sensitized solar cells, and other applications. Phthalocyanines offer high tunability of their electronic and optical properties through the choice of metal center atom; nearly all transition metals and many other heavier elements can reside at the relatively stable phthalocyanine square planar center. The electronic transport properties also depend on the orientation and order of molecular crystals and their chemical environment, making phthalocyanines particularly useful for chemical sensing. In this study, we use angular dependent near-edge x-ray absorption fine structure (NEXAFS) as a quantitative probe of the orientation and electronic structure of H₂-, Fe-, Co-, and Cu-phthalocyanine molecules thin films. NEXAFS measurements at both the carbon and nitrogen K-edges reveal that phthalocyanine films deposited on sapphire have upright molecular orientations, while films up to 50 nm thick deposited on gold substrates are composed of molecules with prostrate orientations. Although great similarity is observed in the carbon and nitrogen K-edge NEXAFS spectra recorded for the films composed of prostrate molecules, the H₂-phthalocyanine exhibits the cleanest angular dependence due to its purely out-of-plane π^* resonances at the absorption onset. In contrast, metal-phthalocyanines have a small in-plane resonance superimposed on this π^* region that is due to a transition into molecular orbitals interacting with the $3d_{x^2-y^2}$ empty state. Complementary NEXAFS spectra recorded at the metal L-edges for the prostrate films reveal dramatic variations in the angular dependence of specific resonances for the Cu-phthalocyanines compared with the Fe-, and Co-phthalocyanines. The Cu L_{3,2} edge exhibits a strong in-plane resonance, due to its b_{1g} LUMO with $d_{x^2-y^2}$ character at the Cu center. Conversely, the Fe- and Co- phthalocyanine L_{3,2} edges have strong out-of-plane resonances arising primarily from LUMO states with e_g symmetry and d_{xz} and d_{yz} character at the metal center.

Introduction:

Thin films of organometallic phthalocyanines (PCs) are versatile device materials—with demonstrated applications in dye-sensitized solar cells¹, organic transistors²⁻⁶, chemiresistive gas-sensors⁷⁻¹⁰, and organic light emitting diodes¹¹. The broad success in implementing this class of planar, organic molecules is a direct consequence of the tunability and sensitivity of their electronic and optical properties with gap energies corresponding to visible wavelengths. In thin film configurations, specified device performance is achieved through a combination of structural selectivity, and the choice of metal center atom. Nearly all transition metals and many heavier elements can reside at the relatively stable square planar center of the phthalocyanine. The metal atom interacts with the ligand, giving rise to a coordination complex with distinct electronic structure.

Building a clear understanding of phthalocyanine electronic structure, especially the nature of metal-ligand interactions, is a fundamental prerequisite to organoelectronic device engineering. Of particular significance are first row transition metal phthalocyanines, including Fe-, Co- and Cu-PCs, where systematic electronic structure changes occur with increasing d-electron filling. Numerous efforts

have been made to characterize and model the electronic structure of these organometallic PCs. Meanwhile, improvements in deposition techniques have enabled experimental studies of highly oriented, thin films (typically <25 nm thick) on a variety of single crystal substrates, *e.g.*, Au¹²⁻²¹. High quality films prepared with advanced deposition techniques have been investigated by a variety of methods, including: x-ray diffraction (XRD)^{22,23}, scanning tunneling microscopy (STM)²⁴⁻²⁶, inverse photoemission spectroscopy (IPES)^{20,27,28}, x-ray photoemission spectroscopy (XPS), ultra-violet photoemission spectroscopy (UPS), and near-edge x-ray absorption fine structure (NEXAFS)^{13-15,18,21,29-33}. Of these experimental methods, NEXAFS has consistently demonstrated success in revealing both local electronic structure (*i.e.*, unoccupied molecular orbitals) and the orientation of condensed molecular films^{15,16,21,29,30,34-40}. Thin films of PCs with highly controlled relative molecular orientation, with respect to the chosen substrate, are ideal candidates for NEXAFS. The planar geometry and sp² bonding of the PC molecules leads to transition dipole moments that are out-of-plane for the π^* orbitals, and in-plane for the C-C and C-N σ^* orbitals (see Fig. 1). When coupled with the use of linearly polarized synchrotron soft x-rays, these distinct transition dipole moment orientations result in strong angular anisotropy of the C 1s and N 1s (K-edge) x-ray absorption resonance intensities for PC films with well-defined molecular orientation. By examining this angular dependence, the orientations of PC molecules are revealed. Due to the valuable structural information available from NEXAFS experiments at the C and N K-edges, the majority of prior studies of PC films have focused upon measurements at these edges. In contrast, comparatively few experiments have been reported for the metal 2p (L-edges) NEXAFS, particularly studies which comprehensively combine the angular dependence of the L_{3,2}-edge spectra with the electronic and orientational information gained from the C and N K-edges. To address this deficiency, a complete collection of angular dependent NEXAFS at the C K-edge, N K-edge and metal L_{3,2}-edges are concurrently acquired on a series of highly oriented H₂- Fe-, Co-, and Cu- phthalocyanine thin films to determine the electronic structure near the metal center.

Theoretical efforts, including a number of detailed *ab initio* calculations, are largely complementary to these data^{28,31-33,41-49}; however, relatively little work has been conducted to extract explicit x-ray absorption cross-sections required to predict angular-dependent NEXAFS. This study combines the data acquired from ordered films with a robust theoretical analysis using a bespoke implementation of the StoBe Density Functional Theory (DFT) package to generate anisotropic x-ray absorption cross-sections and model the angular dependent NEXAFS at the C K-edge, N K-edge and metal L₃-edge.

Experimental:

All organometallic PCs [Fig. 1] were purchased from Sigma Aldrich, and purified several times in a gradient sublimation system, pumped to $\sim 1 \times 10^{-6}$ Torr and heated to 400°C in cycles of 24 hours.⁵⁰ Thin films of PCs were deposited in an organic molecular beam deposition system. This deposition system is contained within a UHV chamber with base pressure $< 1 \times 10^{-10}$ Torr. Purified PCs were loaded into quartz crucibles in Knudsen cells and evaporated at temperatures between 300 and 450°C. Deposition rates of 0.3-0.4 Å/s were achieved by adjusting the temperature and calibrated with a quartz crystal microbalance thickness monitor. Deposited PC thin films were 50 nm thick. Substrates were (0001) cut sapphire; Au coated substrates were prepared by evaporating 40 nm Au onto sapphire and annealing at 300°C for three hours to decrease surface roughness and promote grain enlargement.⁵⁰ Substrates were azimuthally rotated continuously during deposition to ensure uniform films.⁵⁰

NEXAFS data were acquired at beamline 8.0 of the Advanced Light Source (ALS) and at beamline 8.2 at the Stanford Synchrotron Radiation Laboratory. At the ALS, the beam spot was defocused to about 4 mm² in order to reduce flux and associated beam-induced degradation. No beam damage was observed in the samples in the timeframe required to acquire the spectra. Total electron yield (TEY) spectra were acquired by measuring the sample drain current. All TEY spectra were normalized both to a concurrent, upstream, Au flux monitor, and subsequently to the intensity of the absorption step-edge. Total fluorescent yield (TFY) and Auger electron yield (AEY) were also measured, but are not shown for brevity. The AEY, TEY and TFY detection modes have depth sensitivities of Ångströms, nanometers and hundreds of nm, respectively. All detection methods with varying depth sensitivity yielded NEXAFS data with similar angular-dependent intensity changes, indicating our substrates and deposition techniques led to uniform orientational arrangement throughout the films.

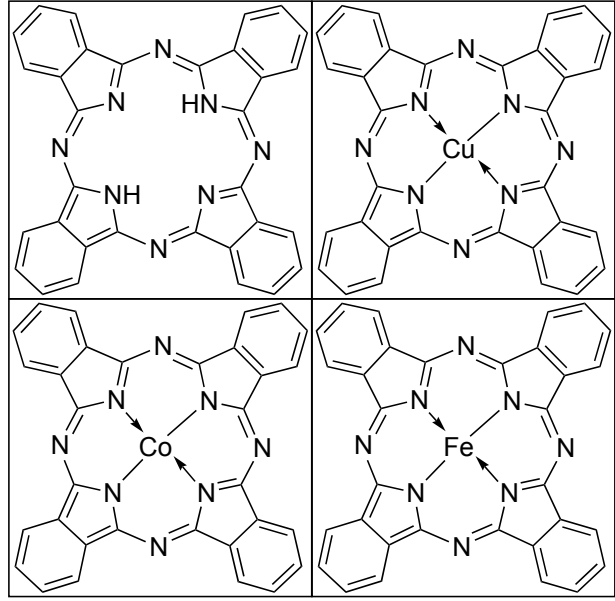


Figure 1: Phthalocyanines under investigation in this study vary only by the choice of species at the center of the square, planar molecule. Thin films of H₂-, Cu-, Co-, and Fe- PCs were found to have a high degree of orientational order. The σ^* lie in-plane along C-H, C-C, and C-N bonds, while the π^* resonances are normal to the molecular plane.

NEXAFS Analysis:

The mean spatial orientation of molecular films can be approximated through analysis of angular dependence in NEXAFS that arises from anisotropy in the transition probability for particular resonances. For PCs this is especially apparent for the C and N K-edge π^* and σ^* resonances where, for example, the 1s to π^* transition dipole moment is approximated by a single vector orthogonal to the phthalocyanine molecular plane²⁸, and can lead to an estimation of the molecular orientation through the relationship^{28,29}

$$\frac{I_v(\theta_i, A)}{I_v(\theta_j, A)} = \frac{P(3A - 1)\theta_i - A + 1}{P(3A - 1)\theta_j - A + 1} \quad (\text{eqn. 1})$$

with

$$\theta = \cos$$

θ^2 , where θ is x-ray incidence angle, with normal to the surface being 90°, $A = \cos(\alpha)^2$, where α is the angle between the π^* vector and the surface normal, and P is the degree of linear polarization defined with respect to the p - and s - components of the incident the x-ray electric field²⁸:

$$P = \frac{E_p^2}{E_p^2 + E_s^2} \quad (\text{eqn. 2})$$

$I_p(\Theta_i, A)$ and $I_p(\Theta_j, A)$ are intensities of a particular π^* resonance acquired at two different incident angles, Θ_i and Θ_j , and appear as a ratio in order to cancel both the intrinsic and experimental polarization-independent cross-section of the resonance. In practice, equation 1 is a linear function of Θ_i , using any chosen and fixed Θ_j . The least-squared fitted slope of $\frac{I_p(\Theta_i)}{I_p(\Theta_j)}$ as a function of Θ_i compared to the theoretical slope from (eqn. 1) which is $\frac{P(3A-1)}{P(3A-1)\Theta_j - A + 1}$. One can solve for A and thus extract the molecular orientation. A similar method can be used for the σ^* resonances, where transition dipoles lie in the molecular plane of PCs using the relationship^{28,29}:

$$\frac{I_p(\Theta_i, \Gamma)}{I_p(\Theta_j, \Gamma)} = \frac{P(3\Gamma - 1)\Theta_i - \Gamma - 1}{P(3\Gamma - 1)\Theta_j - \Gamma - 1} \quad (\text{eqn. 3})$$

with the added complexity that the resonances must be deconvolved from other features (*e.g.*, the step-edge) in the spectra.

First Principles Calculations:

The StoBe DFT code²⁵ enables simulation of the x-ray absorption, the angular dependence of the intensities of NEXAFS resonances, as well as assignment of the unoccupied / final-state orbitals responsible for the NEXAFS resonances. In condensed films of PCs, inter-molecular forces consist primarily of weak van der Waals interactions; consequently, the ensemble is closely approximated by application of DFT to isolated PCs. To model the C and N K-edges, the standard StoBe approach is used to calculate the absorption from each respective atomic center by placing an extended and diffuse `iii_iglo` basis set on an atom of interest and a pseudopotential, approximating the two 1s core electrons, on all other atomic centers, as commonly implemented in StoBe XAS.⁵¹ The computation of the x-ray spectrum at each atomic center required three steps: (1) relaxation of the molecular structure, and computation of the ground state; (2) calculation of the transition potential (TP), in which incorporation of a fractional (usually $\frac{1}{2}$) electronic charge in the alpha spin state of the 1s core-electron was used to compute the profile of the x-ray absorption, statically approximating the dynamic initial and final state; and (3)

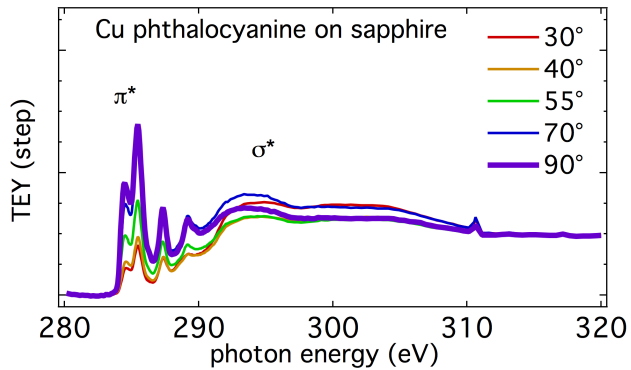


Figure 2: Carbon NEXAFS from Cu phthalocyanine on sapphire. The two most prominent π^* resonances, about 284.5 and 285.5 eV are most intense at normal incidence, least at grazing, indicating an upright orientation of the phthalocyanines.

recomputation of the energy levels with a core-hole in the alpha spin state of the 1s, and an electron in what was the LUMO of the ground state. Finally, the energy scale of the TP computed spectra was adjusted such that the energy of the first resonance matched the overall energy difference between the core-hole state and ground state.⁵¹ No further adjustments were made to the energy scales.

Angular dependence of the intensities of NEXAFS resonances was simulated using the `xrayspec` utility included in the StoBe package along with an auxiliary, self-written code to compute electric field vectors for each angle of incidence and atomic center. Molecular three-fold azimuthal symmetry is sufficient to compute spectra with multiple azimuthal orientations and domain sizes much smaller than the experimental

x-ray beam spot.²⁸ For a given polar molecular orientation and angle of x-ray incidence (with respect to the substrate surface), electric field vectors were calculated and fed into the xrayspec code. The results were summed over all C (or alternatively all N) centers to obtain the angular-dependent NEXAFS spectra.

Modeling of the metal L-edges in Co-, Fe-, and Cu- PCs with StoBe proved to be somewhat more

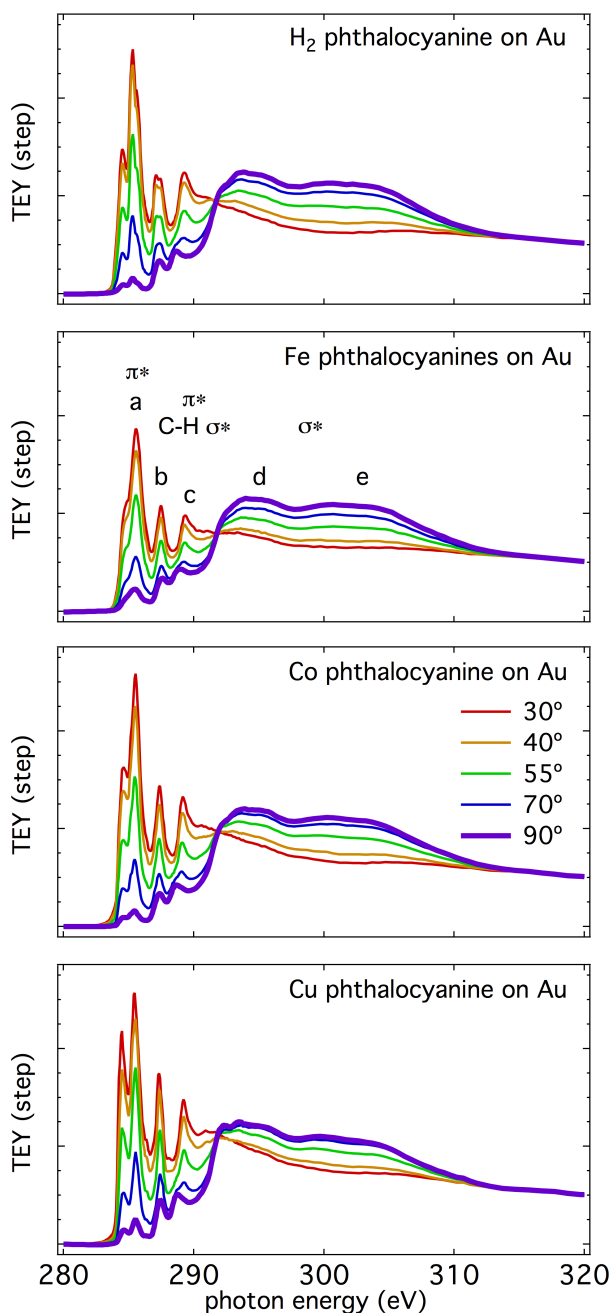


Figure 3: Carbon K-edge NEXAFS from, top to bottom, H₂, Fe, Co, and Cu phthalocyanines on Au. All exhibit π^* resonances that are least intense at normal incidence, and most intense at grazing incidence. Combined with the converse behavior of the σ^* resonances, the NEXAFS indicates, in these cases on Au, the planar molecules lie prostrate on the substrates.

challenging. Other methods are often used to compute x-ray spectra from higher-Z atomic centers⁵²⁻⁵⁵; however, StoBe, which is a real-space, Gaussian-type-orbital code proved adequate to illuminate the nature of the unoccupied orbitals responsible for the most prominent experimentally observed resonances and the dependence of their intensities on the angle of incidence between the molecule and the x-ray beam. The approach was to assign the three 2p alpha orbitals an occupation of 0.833 to give an overall occupation of about $\frac{1}{2}$ of an electronic charge for the TP computation.⁵⁶ The angular dependence and/or orbital overlap between the occupied and unoccupied states is expected to be different whether the initial state is an in-plane orbital (p_x or p_y) or an out-of-plane (p_z) orbital, and therefore, all three p-orbital orientations were explicitly included in the computed x-ray absorption. Further, the most likely oxidation state and electronic structure in square-planar Cu phthalocyanine is well established to be Cu^{2+} with a singly occupied $b_{1g} / d_{x^2-y^2}$ at the HOMO and LUMO.⁵⁷ We found the most straightforward method to ensure proper convergence of the SCF calculation, including ensuring an empty LUMO state in odd-electron system in this particular state, was to compute the Cu and Co L-edges as a molecular cation; otherwise, filling of orbitals by energetic ordering often left this orbital filled. The results of our approach, especially in the case of Cu-phthalocyanine, matched experimental spectra remarkably well. Qualitatively matching the computed to the experimental N K-edge for the Cu-phthalocyanine required adjusting both the overall charge on the molecule as well as the fractional core-level charge; this affected the occupation of the b_{1g} state, but the remainder of the angular-dependent π^* and σ^* features were qualitatively similar.^{40,58}

Results:

Figure 2 presents representative C K-edge NEXAFS spectra for Cu-phthalocyanine

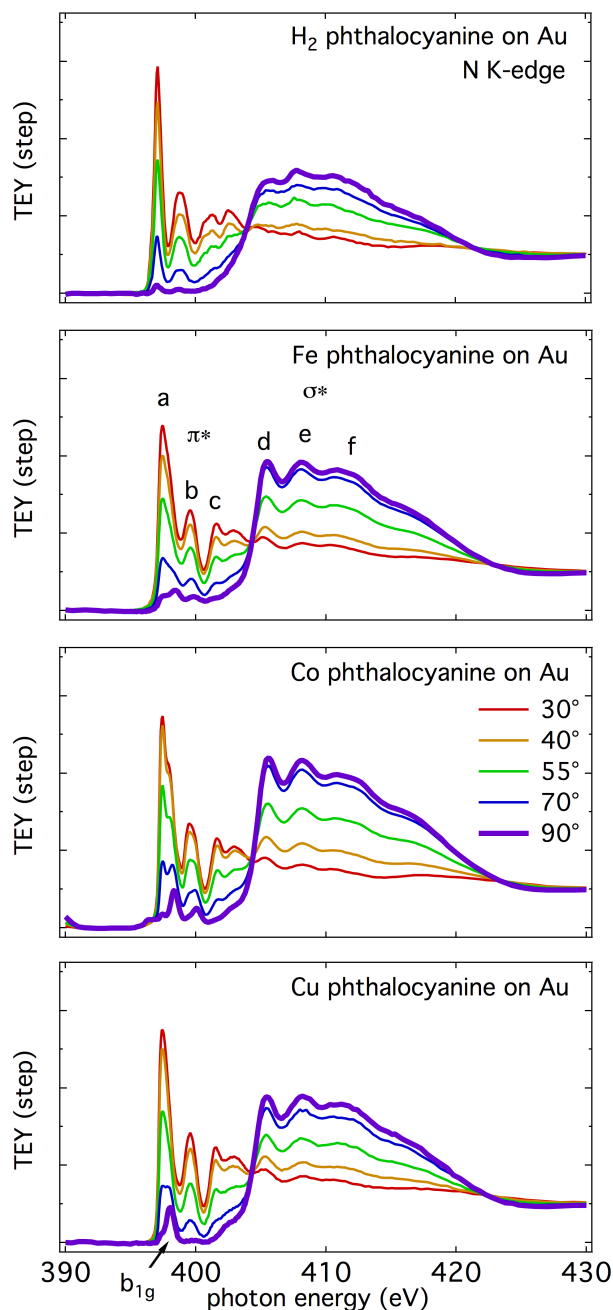


Figure 4: Nitrogen K-edge NEXAFS spectra for each of the H₂, Fe, Co, and Cu phthalocyanine thin films on Au show strong angular dependence that is very similar to the C K-edge spectra.

0° is within one standard deviation of the fit of the slope. Further, the Co-, Fe-, and Cu- phthalocyanines on Au have slightly higher NEXAFS resonance intensities in this π^* region at normal incidence, returning 20° orientation for the π^* transition dipole moment, with a completely flat orientation just outside of one standard deviation on the fit of the slope, yet well within two standard deviations. In any case, the

deposited on sapphire as a function of the angle of x-ray incidence with respect to the sapphire surface. These spectra are representative of others we have measured. In this case, the intensities of the two prominent π^* resonances (labeled) are more intense at normal incidence than at grazing incidence. Analysis of these π^* resonance intensities yields transition dipole moments that exceed 70° with respect to the sapphire surface normal. As these π^* resonances have transition dipole moments that are perpendicular to the phthalocyanine plane, this analysis indicates an upright orientation that is, on average, within 20° of the surface normal for the Cu-phthalocyanine when deposited on sapphire.

Figure 3 presents representative C K-edge NEXAFS spectra for the four investigated phthalocyanines prepared on Au substrates. Each contains two prominent π^* resonances (a in Fig.3) at about 284.5 and 285.5 eV. In contrast with figure 2, these π^* resonances are most intense at grazing incidence, where the electric field of the incident radiation is near normal to the surface and PC thin film. Several additional features at energies just below the absorption edge (287 – 290 eV, b & c) likely have contributions from both π^* states and C-H bonding. Above the absorption edge (~291.8 eV), the spectra from carbonaceous molecules are generally dominated by in-plane C – C and C - N σ^* features (d & e). The σ^* features in figure 3 are generally most intense at normal incidence, and least prominent at grazing incidence. All resonances consistently monotonically increase (π^*) or decrease (σ^*) as the x-ray incidence angle is adjusted from normal to grazing, suggesting high fidelity in these measurements.

The NEXAFS spectra presented in figure 3 indicate that the phthalocyanines deposited on Au have prostrate orientations. For example, analysis of NEXAFS of H₂ phthalocyanine films on Au, by taking the slope from the linear regression of the intensity ratio (eqn. 1), yields about 15° for the π^* transition dipole moment, but

resonances indicate a prostrate orientation for each of the four phthalocyanines films prepared on Au in this study.

Figure 4 displays N K-edge NEXAFS spectra for thin films prepared from all four of the phthalocyanine complexes on Au; as expected, there are strong similarities between the N and C K-edge spectra. The π^* resonance manifolds a, b, & c are extremely intense at grazing incidence, while at normal incidence they are strongly attenuated. In the particular case of the H₂-phthalocyanine film, the π^* resonance (a) is nearly two orders of magnitude less intense at normal incidence (90°) than at grazing incidence (30°). These data are consistent with the behavior observed in the C K-edge spectra and provide support for the assignment of a prostrate orientation of the phthalocyanines on the Au substrate.

Unique differences exist in the N K-edge spectra as compared to the C K-edge spectra. The manifold of resonances just below the absorption edge in the N K-edge data (c) are primarily π^* resonances. At most, only two of the eight N atoms, exclusively in the case of H₂-PC, are terminated with H. In contrast, the analogous region (c in Fig. 3) in the C K-edge has a convolution of both π^* and C-H σ^* resonances, resulting in some intensity in this region at normal x-ray incidence. The C-H σ^* resonance intensity arises due to the fact that 50% of the C atoms reside at the perimeter of the PC molecule and, consequently, are bonded to H. All of the PCs contain a manifold of low energy resonances (a) that generally have angular dependence consistent with π^* resonances; however, specifically in the metal PCs, a relatively sharp resonance persists at normal incidence and likely has the opposite angular dependence as compared to the π^* resonances. This feature is evident for each of the Co- and Cu- PCs.

A completely flat and prostrate orientation of all molecules is well within the error (one standard deviation) of the linear fit of eqn. 1 and the N K-edge π^* , with the exception of FePC being within two standard deviations. The d, e, & f deconvoluted σ^* (Fig. 4) also return a highly prostrate orientation. This is in direct contrast and potentially an improvement over previous studies where often a prostrate monolayer at the substrate interface is followed by upright phthalocyanines in thicker films^{9,14,15,21,30}. With the deposition conditions used here, a homogeneously prostrate orientation is measured in phthalocyanine films on Au substrates as seen in the C and N K-edge data. Finally, the resonances above the absorption edge, particularly d, e & f, are more distinct in the metal PC films than with the H₂-PC films; thus, we infer that these resonances are influenced by N orbital overlap with the metals.

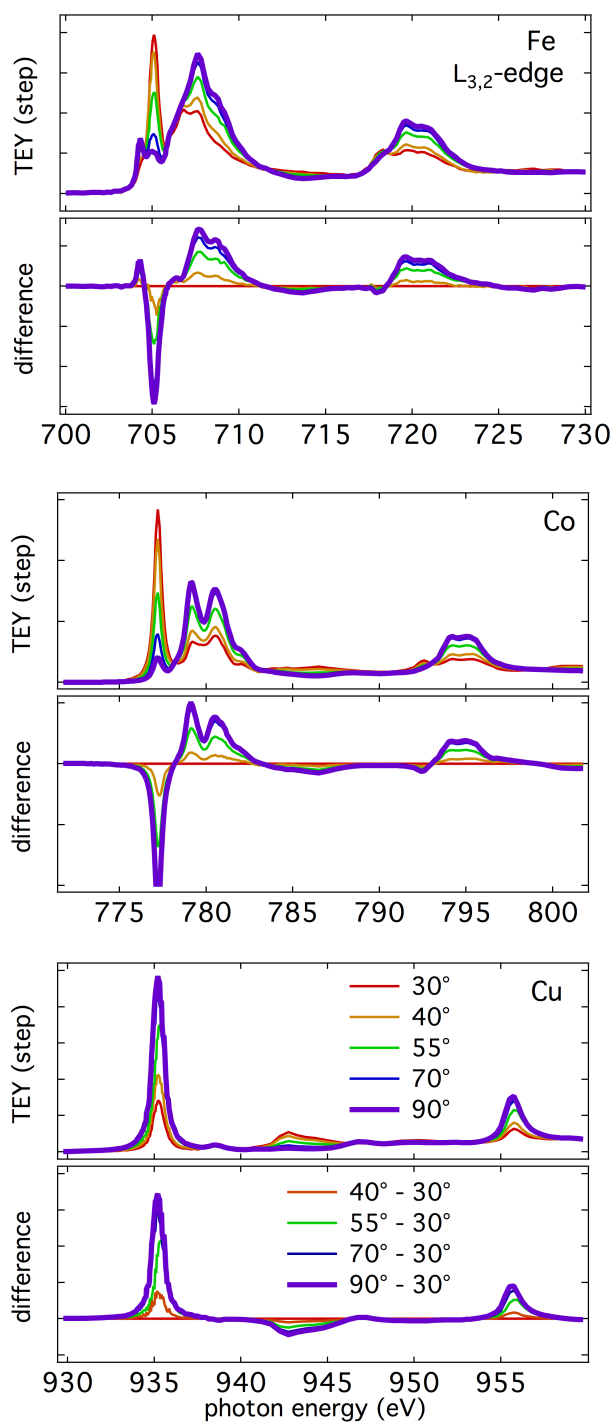


Figure 5: NEXAFS spectra of Metal $L_{2,3}$ -edges from phthalocyanines on Au. Iron, cobalt, and copper are displayed from top to bottom. In each pane, both the total electron yield and difference (subtracting the spectrum acquired at 30 degrees) are presented. The differences are presented to emphasize the angular dependence of the resonances. Note distinctions between Fe, Co, and especially Cu.

NEXAFS data recorded as a function of incidence angle at the metal spin-orbit split $L_{3,2}$ -edges are presented in figure 5. All display strong angular dependence, yet distinct features are apparent between the spectra for the three metal PC films. Both the lower-energy L_3 and higher-energy L_2 portions of the spectra from Fe- and Co-PC films exhibit angular dependence similar to the N and C K-edges: strong resonances at lower energies homologous with C/N π^* resonances, and higher energy, broader resonances analogous to the C-C/N-C σ^* features at both the L_3 - and L_2 -edges. The most pronounced difference between the Fe- and Co- PC NEXAFS spectra is the presence of a single, sharp resonance that appears at the onset of absorption only at the Fe-PC L_3 -edge, which has been attributed to a magnetic state.⁴² In stark contrast with the Fe- and Co- PC data, the Cu-PC spectra shows the first sharp resonance with the opposite angular dependence (strongest at normal incidence, weakest at grazing). About 3.4 eV above this intense resonance appears a barely perceptible peak with slight angular dependence consistent with an out-of-plane resonance. A broader, higher-energy resonance, at about 8 eV above the intense peak, although relatively weakly, also runs counter to the angular dependence of the σ^* resonances of the Fe- and Co- PCs. Even though the Fe-, Co-, and Cu- centers all lie in the same phthalocyanine square-planar environment, the vastly different angular dependence of the NEXAFS clearly indicates different electronic structure and bonding in these three cases.

Discussion:

Angular dependent NEXAFS is an experimental measure of electronic structure; DFT calculations can help interpret and illuminate these data. The StoBe DFT code was used to this end, via simulation of the NEXAFS resonances and their observed angular dependence. Our assignments presented in the following paragraphs both confirm and contradict aspects of various assignments of features in the C K-edge made by previous observations and calculations.^{18,31,40,47,59}

Generally, the most intense π^* resonances in the H_2 -PC also appear in the metal PCs. In the

N K-edge spectra of all four species, the lowest energy, most intense π^* resonance (a in Fig. 4) is comprised of transitions from the 1s to LUMO e_g orbitals. These LUMOs have more electron density at the pyrole rings, but extend lengthwise across the two legs of the molecule. Each of these two orbitals involves all four of the peripheral N atoms, but only two of the interior, and thus, resonances from these atoms are about twice as intense as from the interior N atoms.⁵⁸ The next feature (b in Fig. 4) consists primarily of a convolution of a π^* state, that is delocalized over the entire molecule, and four π^* states at the benzene structures.⁵⁸

Similar π^* resonances appear in the C K-edge spectra; however, the C features are more complex convolution of transitions into unoccupied states shifted in energy by initial and final state differences. Phthalocyanine C can be separated into two groups: pyrole C are within the 5 membered rings and bonded to two N, and benzene C are within the six-membered rings. The most intense C K-edge π^* resonance (a in Fig. 3) is a convolution of the LUMO e_g states excited from pyrole C, and the LUMO+1 states associated with benzene C structures, also excited from these same benzene C. The shoulder/peak at about 1 eV lower energy arises from transitions from benzene C into the LUMO e_g states. The next peak manifold c is an additional π^* state delocalized across much of the molecule. Further, additional states in c are a mix of π^* , as well as σ^* character associated with C-H bonds.⁵⁸

Figure 6 presents StoBe DFT computed NEXAFS spectra for the metal L_3 -edges only, as well as diagrams of the shapes of the molecular orbitals that correspond to the lowest-energy resonances. Although not all of the experimental features and precise energy positions are reproduced, the computed spectra, at least from the standpoint of angular dependence and relative energies, match the experimental data relatively well. Generally, there are two manifolds of peaks, one a few eV higher than the first. The angular dependencies of the Fe- and Co- PC NEXAFS are similar, while the Cu-PC has the opposite angular dependence.

The experimental NEXAFS for the Fe- and Co- PC films on Au shows a strong, out-of-plane transition dipole moment, resembling the π^* resonances observed at the C and N K-edges. The corresponding TP calculations indicate that the Fe-PC has a d_z^2 atomic-like / a_{1g} LUMO orbital and then two e_g orbitals (with d_{xz} and d_{yz} character at the Fe central atom) in the LUMO+1; one of these calculated orbitals is shown beneath the Fe computed spectrum⁵⁸ in figure 6. All three orbitals, according to the calculation, contribute to the intensities of these lowest-energy resonances. Co-PC has two similar e_g (d_{xy}/d_{xz}) orbitals at the LUMO in the TP calculation that are responsible for its lowest-energy resonance. Both Fe- and Co- PCs thus have computed e_g orbitals that have d_{xz} and d_{yz} character near the metal center; these have been referred to as d- π because of the strong orbital overlap.⁴³ Although the transition dipole moments of L-edges are generally more complex than K-edges due to initial states with p-symmetry, experimentally, these particular 2p to 3d resonances, probed with linearly polarized x-rays (Fig. 5), have angular dependence resembling the C and N 1s to molecular π^* states (Figs. 3 and 4).

In stark contrast to the Fe- and Co- L-edges, the Cu has a strong in-plane resonance near the LUMO. StoBe calculations indicate that resonance is from an unoccupied b_{1g} orbital with $d_{x^2-y^2}$ character at the Cu atom; this orbital is also depicted below the computed spectra in figure 6.

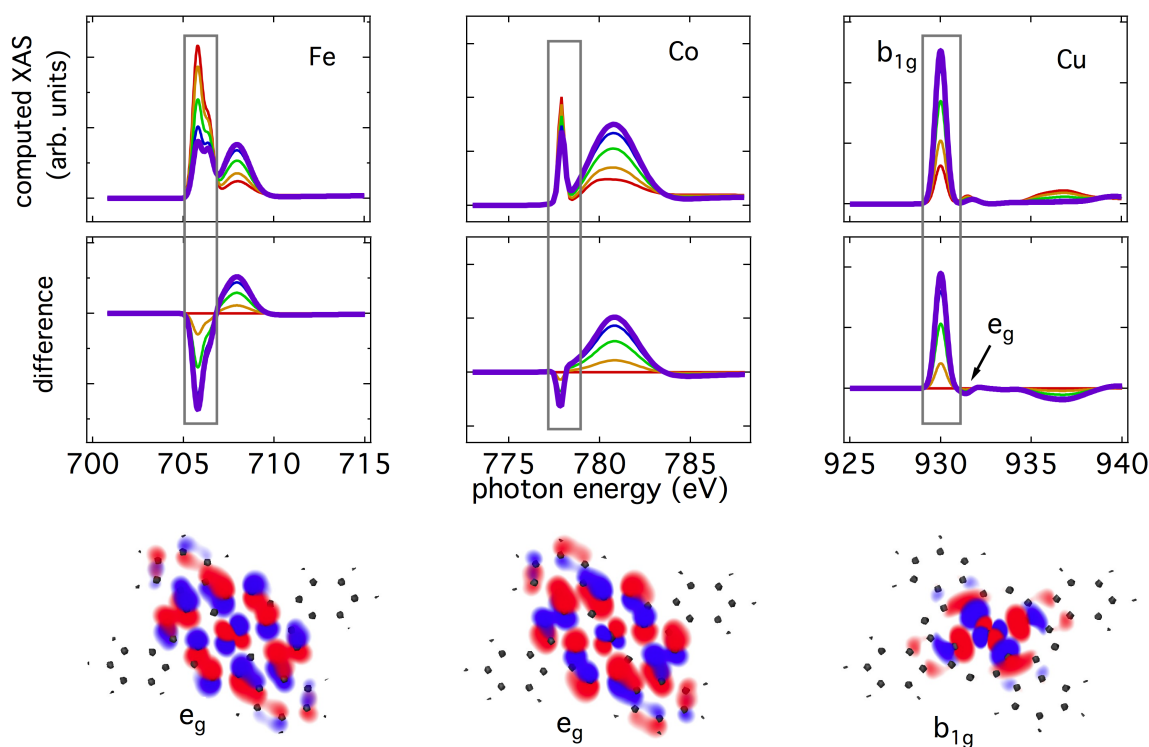


Figure 6: StoBe computed L_3 edges for Fe, Co, and Cu phthalocyanines, as well as representative molecular orbitals responsible for the lowest-energy resonances.

The Cu $2p$ to $d_{x^2-y^2}$ assignment in phthalocyanines (and related molecules) is not without precedent; however, previous investigations neither distinguished this resonance from the most intense C and/or N $1s$ to π^* transitions^{31,57,60}, nor specifically looked experimentally for this resonance in both N K-edges and Cu $L_{3,2}$ edges simultaneously.^{38,47} Also, a relatively weak, but energetically sharp resonance at about 398.4 eV in the N NEXAFS (Fig. 4) persists at normal incidence in the metal PCs. This state has angular dependence that leads to the highest intensity at normal incidence, weakest at grazing, pointing to an in-plane transition dipole. This resonance is due to excitations from the N $1s$ into this $b_{1g} / d_{x^2-y^2}$ state^{38,58}. This resonance also appears in the Fe and Co PCs (see Fig. 4). The energy position of this peak does not change as dramatically with metal atomic number in the experimental NEXAFS data compared to both our StoBe⁵⁸ XAS simulations and other ground-state calculations.⁴³

The relative energy positions of the resonances into e_g and b_{1g} are different depending on the core-level. The very small resonance in the Cu L_3 edge, about 3.2 eV above the intense resonance into b_{1g} , corresponds to the small resonance also seen in the computed data attributed to the e_g state. The experimental energy positions are swapped: in the CuPC N K-edge, the b_{1g} lies 0.4 and 0.7 eV above the two peaks fit to the lowest-energy π^* ⁵⁸; the b_{1g} in the Cu L_3 edge lies 3.3 eV below the peak assigned to the e_g . This difference can only be due to the inherently dynamic Cu $2p$ and N $1s$ electron promotion and associated electron screening.

Conclusions:

Experimental and theoretical analysis of x-ray absorption in ordered thin films of H_2 -, Fe-, Co-, and Cu-phthalocyanines at the C and N K-edges, and the respective metal L-edges has provided both the preferred molecular orientation within these condensed films and a complete description of the associated electronic structure. Angular dependence in the C and N K-edge NEXAFS of all the PC films investigated show that, on Au substrates, these PCs lay prostrate on the surface. The Fe, Co, and Cu L-

edge NEXAFS also show strong angular dependence, but vary significantly between the three species. Iron and cobalt PCs have angular dependence that resembles the C and N K-edges, with $d-\pi^*$ states dominating the lowest unoccupied orbitals; conversely, the Cu L-edge shows its lowest unoccupied orbitals having the opposite angular dependence, and thus a transition dipole moment that is in-plane with the PC molecule. Stobe DFT calculations indicate that this converse angular dependence in the metal L-edge NEXAFS arises because the lowest energy resonance corresponds to the excitation of an electron into an unoccupied state within the molecular plane for the Cu-PC (specifically the b_{1g} orbital which has $d_{x^2-y^2}$ character at the Cu atom), versus an unoccupied state that is oriented perpendicular to the molecular plane for the Fe- and Co- PC (the e_g orbitals which have d_{xz} and d_{yz} character). The b_{1g} state also appears in the N K-edge NEXAFS as an in-plane resonance that is relatively weak compared to the π^* resonance.

Acknowledgements:

Portions of this work performed under the auspices of the U.S. Department of Energy by Lawrence Livermore National Laboratory under Contract DE-AC52-07NA27344. The Advanced Light Source is supported by the Director, Office of Science, Office of Basic Energy Sciences, of the U.S. Department of Energy under Contract No. DE-AC02-05CH11231. Portions of this research were carried out at the Stanford Synchrotron Radiation Lightsource, a Directorate of SLAC National Accelerator Laboratory and an Office of Science User Facility operated for the U.S. Department of Energy Office of Science by Stanford University. This work supported by a University of California Office of the President (UCOP) Management Fee Grant, "Carbon Nanostructures". The authors acknowledge Juan Bartolome, Franz Himpsel, Xiaosong Liu, and Ioannis Zegkinoglou for useful discussions.

References

- (1) MacNaughton, J. B.; Moewes, A.; Lee, J. S.; Wettig, S. D.; Kraatz, H. B.; Ouyang, L. Z.; Ching, W. Y.; Kurmaev, E. Z. *J Phys Chem B* **2006**, *110*, 15742.
- (2) Yang, R. D.; Gredig, T.; Colesniuc, C. N.; Park, J.; Schuller, I. K.; Trogler, W. C.; Kummel, A. C. *Appl Phys Lett* **2007**, *90*, 263506.
- (3) Yang, R. D.; Park, J.; Colesniuc, C. N.; Schuller, I. K.; Trogler, W. C.; Kummel, A. C. *J Appl Phys* **2007**, *102*, 034515.
- (4) Aristov, V. Y.; Molodtsova, O. V.; Ossipyan, Y. A.; Doyle, B. P.; Nannarone, S.; Knufer, M. *Org Electron* **2009**, *10*, 8.
- (5) Park, J.; Royer, J. E.; Colesniuc, C. N.; Bohrer, F. I.; Sharoni, A.; Jin, S. H.; Schuller, I. K.; Trogler, W. C.; Kummel, A. C. *J Appl Phys* **2009**, *106*, 034505.
- (6) Yang, R. D.; Park, J.; Colesniuc, C. N.; Schuller, I. K.; Royer, J. E.; Trogler, W. C.; Kummel, A. C. *J Chem Phys* **2009**, *130*, 164703.
- (7) Miller, K. A.; Yang, R. D.; Hale, M. J.; Park, J.; Fruhberger, B.; Colesniuc, C. N.; Schuller, I. K.; Kummel, A. C.; Trogler, W. C. *J Phys Chem B* **2006**, *110*, 361.
- (8) Bohrer, F. I.; Sharoni, A.; Colesniuc, C.; Park, J.; Schuller, I. K.; Kummel, A. C.; Trogler, W. C. *J Am Chem Soc* **2007**, *129*, 5640.
- (9) Bohrer, F. I.; Colesniuc, C. N.; Park, J.; Schuller, I. K.; Kummel, A. C.; Trogler, W. C. *J Am Chem Soc* **2008**, *130*, 3712.
- (10) Bohrer, F. I.; Colesniuc, C. N.; Park, J.; Ruidiaz, M. E.; Schuller, I. K.; Kummel, A. C.; Trogler, W. C. *J Am Chem Soc* **2009**, *131*, 478.
- (11) MacNaughton, J. B.; Yablonskikh, M. V.; Hunt, A. H.; Kurmaev, E. Z.; Lee, J. S.; Wettig, S. D.; Moewes, A. *Phys Rev B* **2006**, *74*, 125101.

- (12) Biswas, I.; Peisert, H.; Schwieger, T.; Dini, D.; Hanack, M.; Knupfer, M.; Schmidt, T.; Chasse, T. *J Chem Phys* **2005**, *122*, 064710.
- (13) Biswas, I.; Peisert, H.; Zhang, L.; Chasse, T.; Knupfer, M.; Hanack, M.; Dini, D.; Schmidt, T.; Batchelor, D. *Mol Cryst Liq Cryst* **2006**, *455*, 241.
- (14) Peisert, H.; Biswas, I.; Zhang, L.; Knupfer, M.; Hanack, M.; Dini, D.; Batchelor, D.; Chasse, T. *Surf Sci* **2006**, *600*, 4024.
- (15) Biswas, I.; Peisert, H.; Nagel, M.; Casu, M. B.; Schuppler, S.; Nagel, P.; Pellegrin, E.; Chasse, T. *J Chem Phys* **2007**, *126*, 174704.
- (16) Molodtsova, O. V.; Aristov, V. Y.; Zhilin, V. M.; Ossipyan, Y. A.; Vyalikh, D. V.; Doyle, B. P.; Nannarone, S.; Knupfer, M. *Appl Surf Sci* **2007**, *254*, 99.
- (17) Molodtsova, O. V.; Knupfer, M.; Ossipyan, Y. A.; Aristov, V. Y. *J Appl Phys* **2008**, *104*.
- (18) Calabrese, A.; Floreano, L.; Verdini, A.; Mariani, C.; Betti, M. G. *Phys Rev B* **2009**, *79*, 115446.
- (19) Grobosch, M.; Aristov, V. Y.; Molodtsova, O. V.; Schmidt, C.; Doyle, B. P.; Nannarone, S.; Knupfer, M. *J Phys Chem C* **2009**, *113*, 13219.
- (20) Jie, X.; Peter, A. D. *Journal of Physics: Condensed Matter* **2009**, *21*, 052001.
- (21) Peisert, H.; Biswas, I.; Knupfer, M.; Chasse, T. *Phys Status Solidi B* **2009**, *246*, 1529.
- (22) Miller, C. W.; Sharoni, A.; Liu, G.; Colesniuc, C. N.; Fruhberger, B.; Schuller, I. K. *Phys Rev B* **2005**, *72*.
- (23) Liu, G.; Gredig, T.; Schuller, I. K. *Epl-Europhys Lett* **2008**, *83*.
- (24) Wilks, R. G.; Kurmaev, E. Z.; Sandratskii, L. M.; Postnikov, A. V.; Finkelstein, L. D.; Surkova, T. P.; Lopez-Rivera, S. A.; Moewes, A. *J Phys-Condens Mat* **2006**, *18*, 10405.
- (25) Hermann, K.; Pettersson, L. G. M.; Casida, M. E.; Daul, C.; Goursot, A.; Koester, A.; Proynov, E.; St-Amant, A.; Salahub, D. R. *StoBe-deMon version 3.1* **2011**.
- (26) Cheng, Z. H.; Du, S. X.; Guo, W.; Gao, L.; Deng, Z. T.; Jiang, N.; Guo, H. M.; Tang, H.; Gao, H. *Nano Res* **2011**, *4*, 523.
- (27) Yablonskikh, M. V.; Braun, J.; Kuchel, M. T.; Postnikov, A. V.; Denlinger, J. D.; Shreder, E. I.; Yarmoshenko, Y. M.; Neumann, M.; Moewes, A. *Phys Rev B* **2006**, *74*.
- (28) Stöhr, J. *NEXAFS Spectroscopy*; Springer-Verlag: Berlin - Heidelberg - New York, 1992.
- (29) Willey, T. M.; Vance, A. L.; van Buuren, T.; Bostedt, C.; Nelson, A. J.; Terminello, L. J.; Fadley, C. S. *Langmuir* **2004**, *20*, 2746.
- (30) Peisert, H.; Biswas, I.; Zhang, L.; Knupfer, M.; Hanack, M.; Dini, D.; Cook, M. J.; Chambrier, I.; Schmidt, T.; Batchelor, D.; Chasse, T. *Chem Phys Lett* **2005**, *403*, 1.
- (31) Aristov, V. Y.; Molodtsova, O. V.; Maslyuk, V.; Vyalikh, D. V.; Zhilin, V. M.; Ossipyan, Y. A.; Bredow, T.; Mertig, I.; Knupfer, M. *Appl Surf Sci* **2007**, *254*, 20.
- (32) Aristov, V. Y.; Molodtsova, O. V.; Maslyuk, V. V.; Vyalikh, D. V.; Zhilin, V. M.; Ossipyan, Y. A.; Bredow, T.; Mertig, I.; Knupfer, M. *J Chem Phys* **2008**, *128*.
- (33) Cook, P. L.; Yang, W. L.; Liu, X. S.; Garcia-Lastra, J. M.; Rubio, A.; Himpsel, F. J. *J Chem Phys* **2011**, *134*.
- (34) Zhang, L.; Peisert, H.; Biswas, I.; Knupfer, M.; Batchelor, D.; Chasse, T. *Surf Sci* **2005**, *596*, 98.
- (35) Rosa, A.; Baerends, E. J. *Inorganic Chemistry* **1994**, *33*, 584.

- (36) Holland, B. N.; Cabailh, G.; Peltekis, N.; McGuinness, C.; Cafolla, A. A.; McGovern, I. T. *Appl Surf Sci* **2008**, *255*, 775.
- (37) Molodtsova, O. V.; Knupfer, M.; Aristov, V. Y.; Vyalikh, D. V.; Zhilin, V. M.; Ossipyan, Y. A. *J Appl Phys* **2008**, *103*, 053711.
- (38) Holland, B. N.; Peltekis, N.; Farrelly, T.; Wilks, R. G.; Gavrila, G.; Zahn, D. R. T.; McGuinness, C.; McGovern, I. T. *Phys Status Solidi B* **2009**, *246*, 1546.
- (39) Garcia-Lastra, J. M.; Cook, P. L.; Himpfel, F. J.; Rubio, A. *J Chem Phys* **2010**, *133*.
- (40) Linares, M.; Stafstrom, S.; Rinkevicius, Z.; Agren, H.; Norman, P. *J Phys Chem B* **2011**, *115*, 5096.
- (41) Hamilton, T.; Foursa, M.; Hirose, A.; Moewes, A. *Radiat Phys Chem* **2006**, *75*, 1613.
- (42) Bartolome, J.; Bartolome, F.; Garcia, L. M.; Filoti, G.; Gredig, T.; Colesniuc, C. N.; Schuller, I. K.; Cezar, J. C. *Phys Rev B* **2010**, *81*.
- (43) Liao, M. S.; Scheiner, S. *J Chem Phys* **2002**, *117*, 205.
- (44) Lozzi, L.; Santucci, S.; La Rosa, S.; Delley, B.; Picozzi, S. *J Chem Phys* **2004**, *121*, 1883.
- (45) MacNaughton, J. B.; Wilks, R. G.; Lee, J. S.; Moewes, A. *J Phys Chem B* **2006**, *110*, 18180.
- (46) Seo, J. H.; Park, D. S.; Cho, S. W.; Kim, C. Y.; Jang, W. C.; Whang, C. N.; Yoo, K. H.; Chang, G. S.; Pedersen, T.; Moewes, A.; Chae, K. H.; Cho, S. J. *Appl Phys Lett* **2006**, *89*.
- (47) Molodtsova, O. V.; Knupfer, M.; Maslyuk, V. V.; Vyalikh, D. V.; Zhilin, V. M.; Ossipyan, Y. A.; Bredow, T.; Mertig, I.; Aristov, V. Y. *J Chem Phys* **2008**, *129*.
- (48) Maslyuk, V. V.; Aristov, V. Y.; Molodtsova, O. V.; Vyalikh, D. V.; Zhilin, V. M.; Ossipyan, Y. A.; Bredow, T.; Mertig, I.; Knupfer, M. *Appl Phys a-Mater* **2009**, *94*, 485.
- (49) Chang, G. S.; Kurmaev, E. Z.; Finkelstein, L. D.; Babushkina, N. A.; Moewes, A.; Callcott, T. A. *Phys Rev B* **2006**, *74*.
- (50) Colesniuc, C. N., University of California, San Diego, 2011.
- (51) Leetmaa, M.; Ljungberg, M.; Ogasawara, H.; Odelius, M.; Naslund, L. A.; Nilsson, A.; Pettersson, L. G. M. *J Chem Phys* **2006**, *125*.
- (52) Rehr, J. J.; Albers, R. C. *Rev Mod Phys* **2000**, *72*, 621.
- (53) Rehr, J. J.; Kas, J. J.; Vila, F. D.; Prange, M. P.; Jorissen, K. *Phys Chem Chem Phys* **2010**, *12*, 5503.
- (54) Anniyev, T.; Ogasawara, H.; Ljungberg, M. P.; Wikfeldt, K. T.; MacNaughton, J. B.; Naslund, L. A.; Bergmann, U.; Koh, S.; Strasser, P.; Pettersson, L. G. M.; Nilsson, A. *Phys Chem Chem Phys* **2010**, *12*, 5694.
- (55) de Groot, F. *Coordin Chem Rev* **2005**, *249*, 31.
- (56) Wilks, R. G.; MacNaughton, J. B.; Kraatz, H. B.; Regier, T.; Moewes, A. *J Phys Chem B* **2006**, *110*, 5955.
- (57) Dufour, G.; Poncey, C.; Rochet, F.; Roulet, H.; Iacobucci, S.; Sacchi, M.; Yubero, F.; Motta, N.; Piancastelli, M. N.; Sgarlata, A.; DeCrescenzi, M. *J Electron Spectrosc* **1995**, *76*, 219.
- (58) See supporting information.
- (59) Evangelista, F.; Carravetta, V.; Stefani, G.; Jansik, B.; Alagia, M.; Stranges, S.; Ruocco, A. *J Chem Phys* **2007**, *126*.
- (60) Carniato, S.; Luo, Y.; Agren, H. *Phys Rev B* **2001**, *63*.

Supplemental Information

Electronic Structure Differences Between H₂⁻, Fe⁻, Co⁻, and Cu-Phthalocyanine Highly Oriented Thin Films Observed Using NEXAFS Spectroscopy

T. M. Willey¹, M. Bagge-Hansen¹, J. R. I. Lee¹, R. Call^{1, 2}, L. Landt^{1, 3}, T. van Buuren¹, C. Colesniuc⁴, C. M. Monton⁴, I. Schuller⁴

(1) Condensed Matter and Materials Division, Lawrence Livermore National Laboratory, CA, USA

(2) Department of Physics and Astronomy, Utah State University, Logan, UT, USA

(3) Institute for Optics and Atomic Physics, Technische Universität Berlin, Berlin, Germany

(4) Department of Physics, University of California, San Diego, La Jolla, CA, USA

Details on the StoBe Computations Used in the Paper and Supplemental Information

The StoBe code (<http://www.fhi-berlin.mpg.de/KHsoftware/StoBe/>) was used to compute NEXAFS spectra. The atoms were numbered as seen on the figure of this page; H₂-phthalocyanine was computed with hydrogens bound to the N1 and N5 atoms. Ground-state molecules were geometrically optimized, and then the MO's were computed. Transition Potential (TP) computations were carried out, calculating the transition dipole moment intensities between a fictitious half-filled core and empty states; a commonly used static approximation for the dynamic x-ray absorption process. Key parameters used in the StoBe computations:

(For the H₂ phthalocyanine; metal PCs adjusted accordingly and as described elsewhere)

Ground-state:	Transition Potential:	Core-hole:
potential nonlocal pbe pbe	fsym scfocc excited	fsym scfocc excited
grid fine nonrandom	alfa 94	alfa 95
multiplicity 1	beta 94	beta 94
charge 0	sym 1	sym 1
fsym scfocc	alfa 0 1 1 0.5	alfa 0 1 1 0.0
alfa 94	beta 0 0	beta 0 0
beta 94		

For the L-edges,

fsym scfocc excited

alfa 106

beta 106

sym 1

alfa 0 3 3 0.833 4 0.833 5 0.833

beta 0 0

and the StoBe code was modified to compute the x-ray absorption from orbitals 3, 4, and 5 explicitly.

Basis sets and pseudopotentials used:

A-NITROGEN (5,2;5,2) and O-NITROGEN iii_iglo or A-CARBON (5,2;5,2) and O-CARBON iii_iglo

A-CARBON(+4) (3,3;3,3)

A-NITROGEN(+5) (4,4;4,4)

A-HYDROGEN (3,1;3,1)

O-CARBON(+4) (311/211/1)

O-NITROGEN(+5) (321/311/1)

O-HYDROGEN (311/1) misc

P-CARBON(+4) (3,1:8,0)

P-NITROGEN(+5) (5:6)

A-IRON (5,8;5,8)

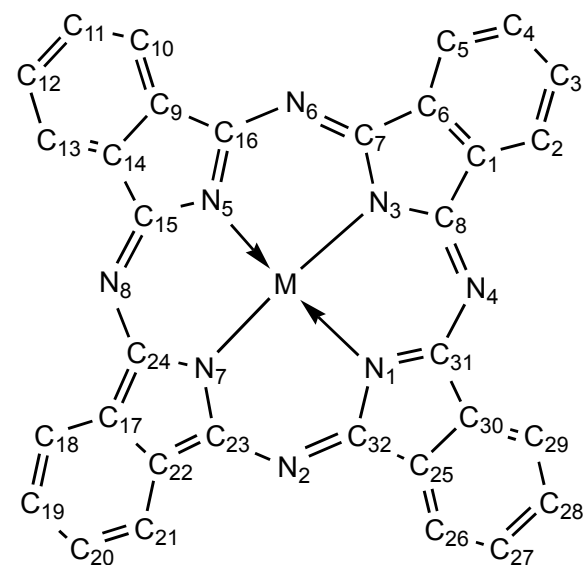
O-IRON (63321/531/311) or O-IRON F-III A

A-COBALT (5,5;5,5)

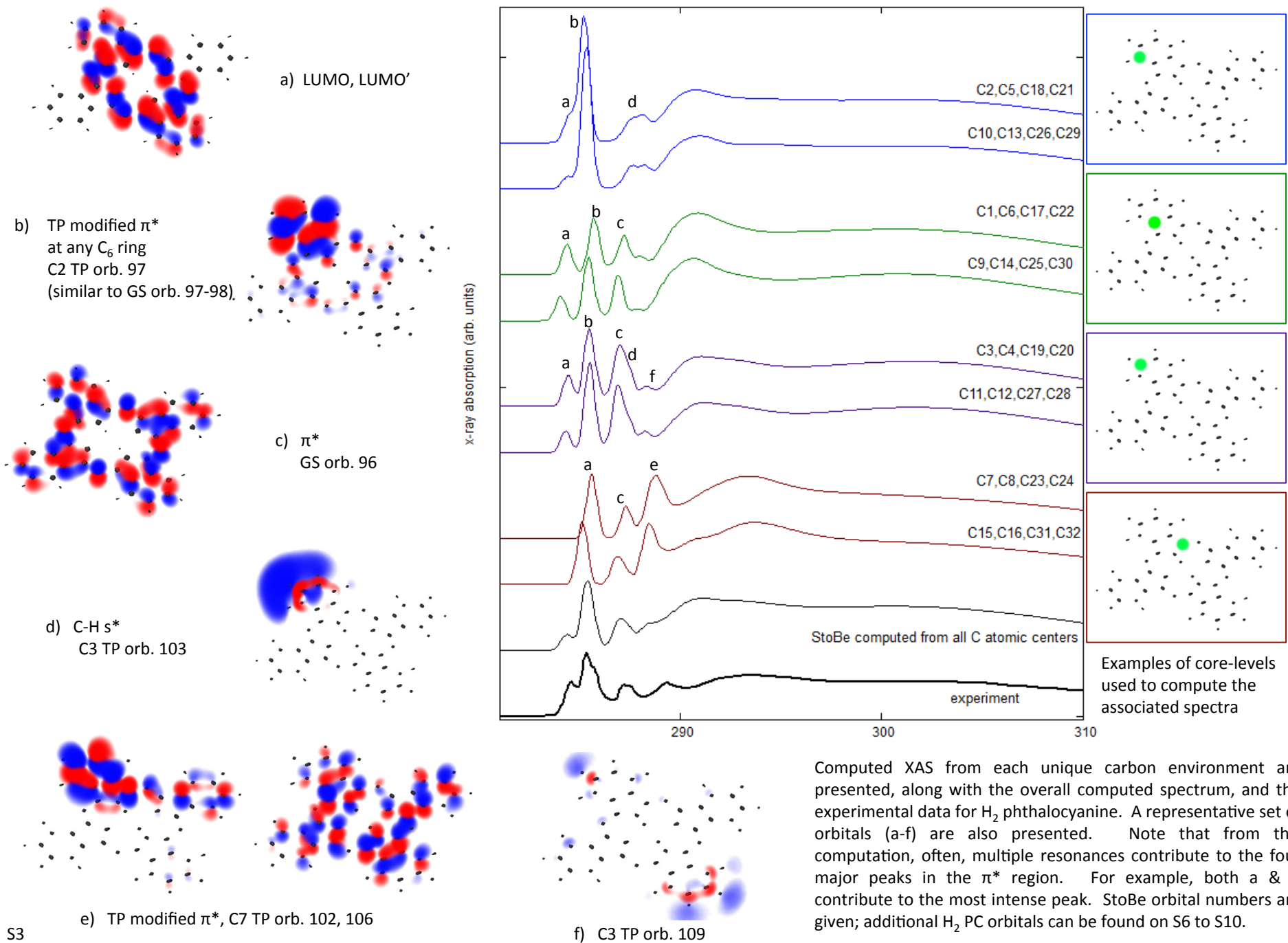
O-COBALT (63321/531/311) or O-COBALT F-III A

A-COPPER (5,8;5,8)

O-COPPER (63321/531/311) or O-COPPER F-III A

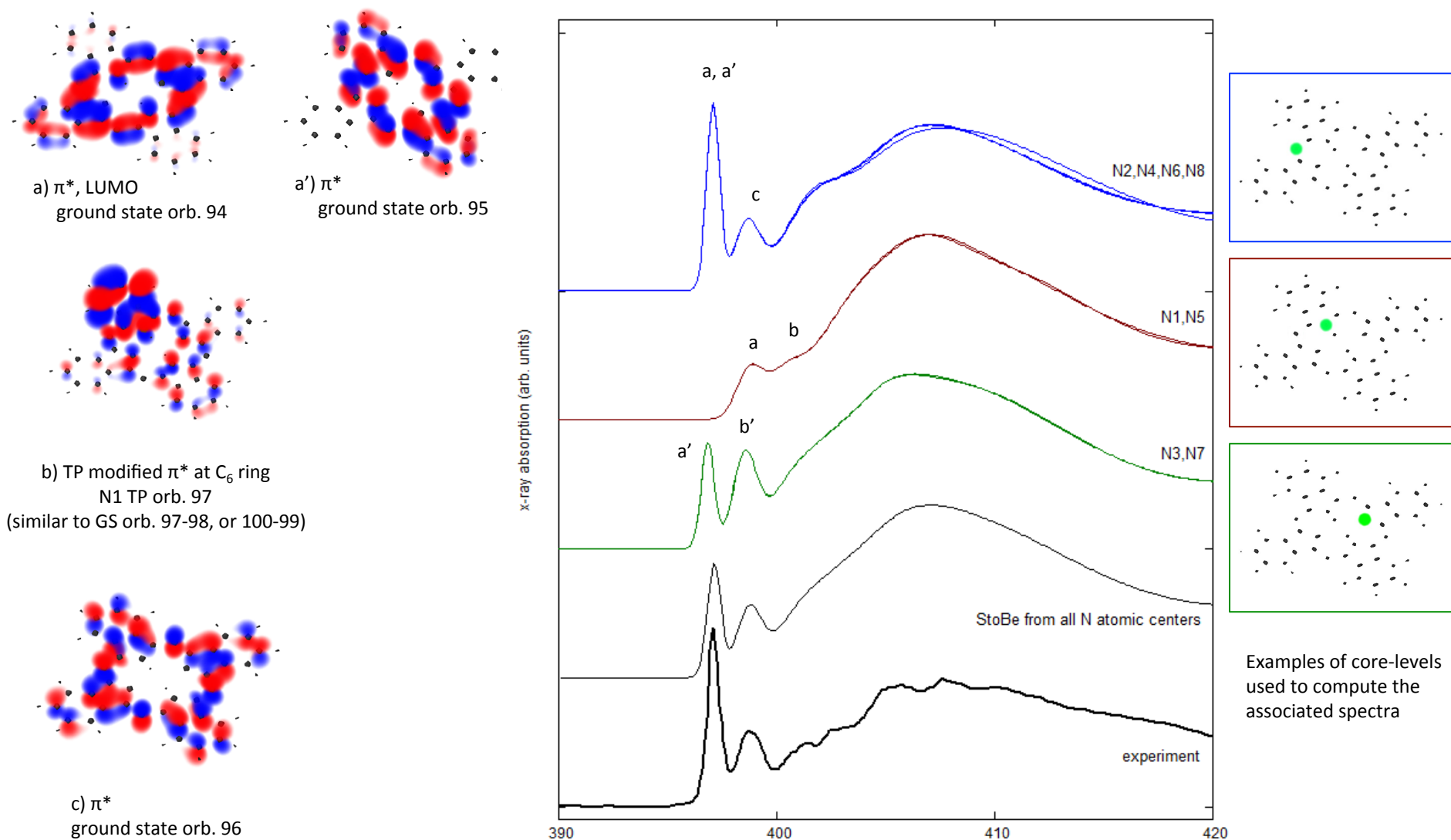


Carbon XAS spectra computed for each unique carbon environment in H₂ phthalocyanine, and the virtual orbitals that lead to the resonances in the XAS



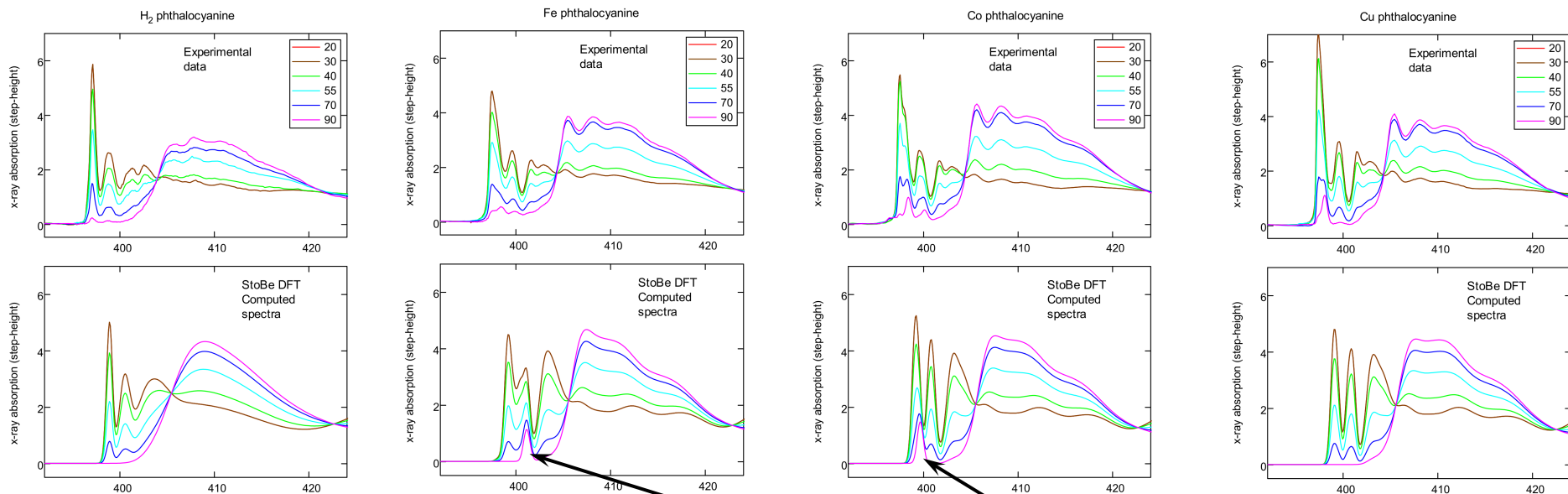
Computed XAS from each unique carbon environment are presented, along with the overall computed spectrum, and the experimental data for H₂ phthalocyanine. A representative set of orbitals (a-f) are also presented. Note that from this computation, often, multiple resonances contribute to the four major peaks in the π^* region. For example, both a & b contribute to the most intense peak. StoBe orbital numbers are given; additional H₂ PC orbitals can be found on S6 to S10.

Nitrogen XAS spectra computed for each unique carbon environment in H₂ phthalocyanine, and the virtual orbitals that lead to the resonances in the XAS



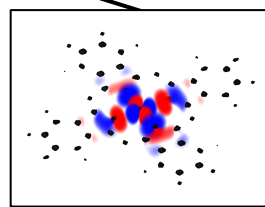
Computed XAS from each unique nitrogen environment are presented, along with the overall computed spectrum, and the experimental data for H₂ phthalocyanine. A representative set of orbitals (a-c) are also presented. Note that from this computation, the most intense, lowest energy π^* is uniquely attributable to the two LUMO orbitals, while the next manifold is a convolution of b, c, and possibly chemically shifted a. These and additional orbitals from the various ground-state (GS) and transition potential (TP) calculations used for obtaining the XAS traces are given on pages S5-S9 for H₂ PC and the metal PCs on pages S11-S17.

Comparison of Experimental and Computed Nitrogen NEXAFS Spectra, and the Computed Orbitals Responsible for the Peaks Indicated

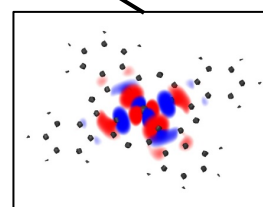


These panes present comparison between experiment and computation, presented in columns, for H_2 , Fe-, Co-, and Cu-phthalocyanine N K-edge NEXAFS. The experimental data is in the first row. Particularly, small peak in what is typically considered a π^* region has a resonance that appears to be in-plane, only in the metal phthalocyanines. This peak is most prominent at normal (90°), and has increasing intensity through the series of Fe-, Co-, and Cu-phthalocyanine.

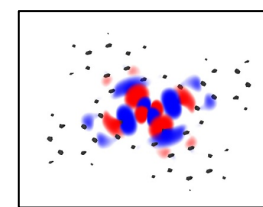
In Fe- and Co-phthalocyanine, this peak is easily seen in the calculation, and attributable to the b_{1g} orbital with $d_{x^2-y^2}$ character near the metal center. In Cu-PC (rightmost column), however, the calculation required some modification. The peak does not appear with a non-physical 0.5 electron in the core-level, 2nd row, nor in the 3rd row where an additional electron is removed from what was the GS HOMO. The core-level fractional charge and associated reduced screening appears to lower the energy of this state to the point where it is occupied in the TP calculation. By increasing the fractional charge placed in the core-level, in this case to 0.9, the state is virtual, and contributes to the computed XAS. Note the variations in the rest of the spectral features of the computed spectra: The intensities and energy positions do change, but the overall features and their associated angular dependence are preserved. In any case, the experimental data clearly contains this in-plane resonance, and the StoBe calculations point to this $b_{1g} / d_{x^2-y^2}$ state as the origin of this peak in these three metal phthalocyanines.



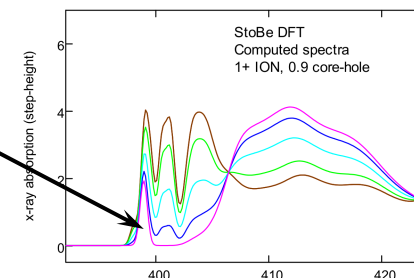
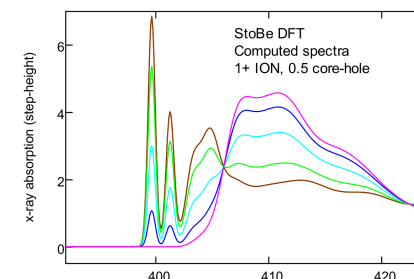
LUMO+3, orb. 110a



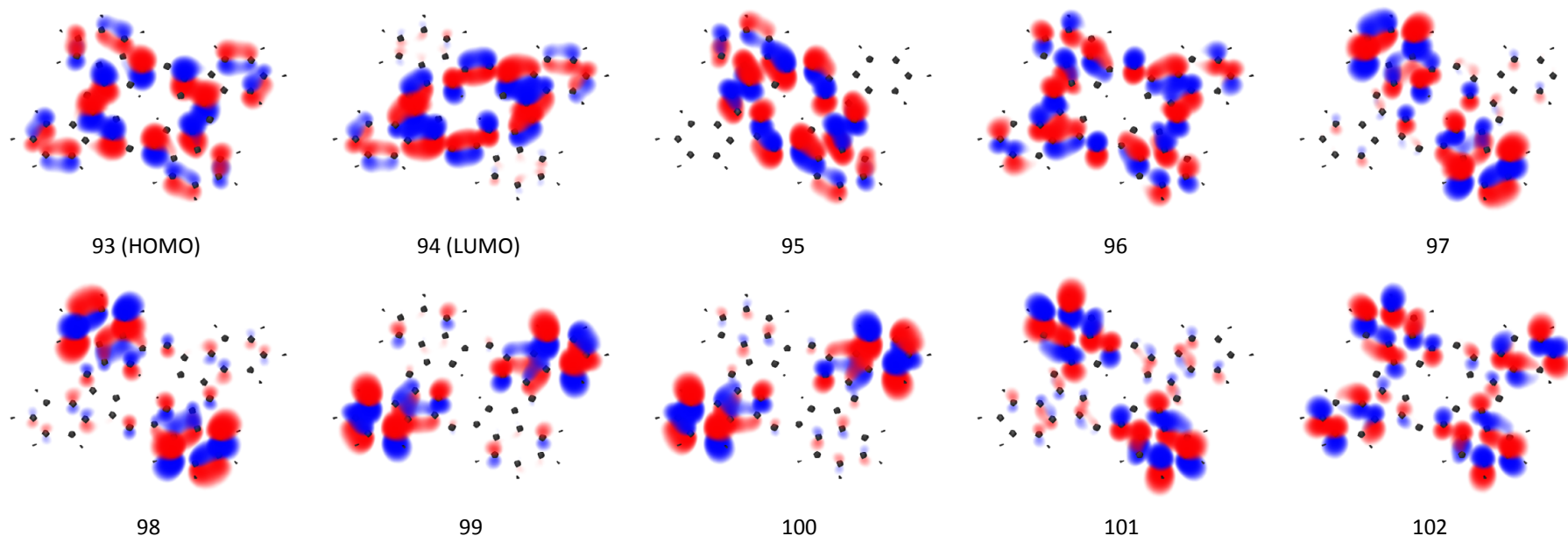
LUMO+2, orb. 110ab



LUMO, orb. 108a



H₂ PC ground state orbitals

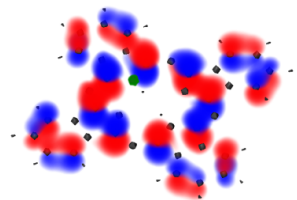


The following pages contain depictions of orbitals computed via StoBe with orbital assignment number under the picture. Looking at these orbitals, the LUMO consists of a π^* resonance concentrated on the 4 peripheral nitrogens and the two interior nitrogens, along with “pyrole carbons” (carbons in the 5-membered rings, but more specifically, carbons not also in the six-membered rings), and some minor electron density on some of the six-membered “benzene carbon” rings. The LUMO (orb. 94 here) and LUMO+1 (orb. 95) have unique energies caused by the interior hydrogens and are not degenerate. In metal phthalocyanines, these are energetically degenerate in the ground state. The LUMO+2 is a π^* extended over most of the molecule, but has almost no electron density at the interior nitrogens and some of the benzene carbons. The next four orbitals are associated with the four benzene rings in the phthalocyanine (97-100) and are followed by several more various π^* orbitals. The following pages are orbitals plotted from the TP calculations indicated; i.e. the actual orbitals used to compute the XAS profile in StoBe.

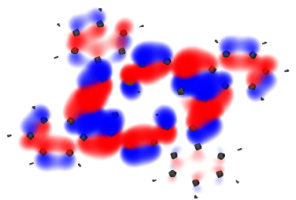
Generally, the half-core-hole static approximation was used, and this will change the electron densities, especially around the core-level of interest, as well as the StoBe orbital numbering scheme with the inclusion of core-electrons in the TP calculations. Note the re-ordering of orbitals energetically when the half-core hole is placed on various nitrogens on the following two pages. For example, the LUMO orbitals for N1 and N3 (orbitals 95 and 96, next page) change position. Also, as energetic positions are close and do change, in some cases, superpositions of the TP orbitals resemble the ground state orbitals presented above, as in the case for the LUMO orbitals in TP calculations for N2 and N4. Shown for the N4 TP calculations are orbitals 95 and 96, whose sum and difference resemble orbitals 94 and 95 in the GS calculation above.

Similar trends are seen in the TP orbitals computed for carbon spectra.

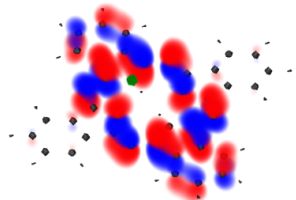
H₂ PC XAS TP calculation, N1 (green)



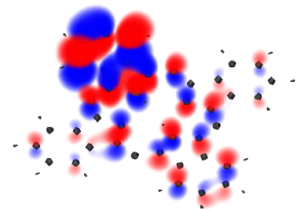
94 (HOMO)



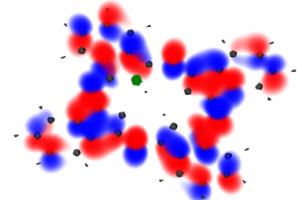
95 (LUMO)



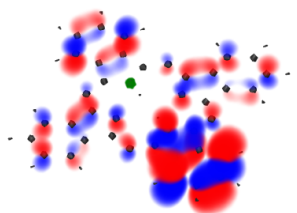
96



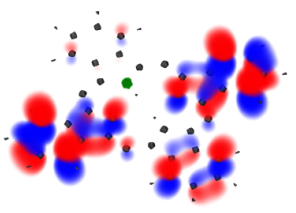
97



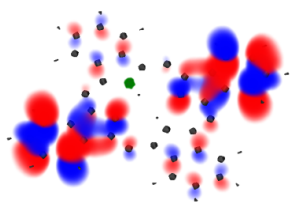
98



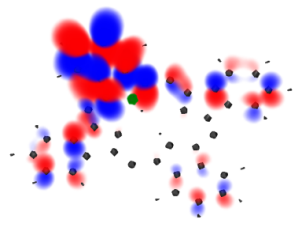
99



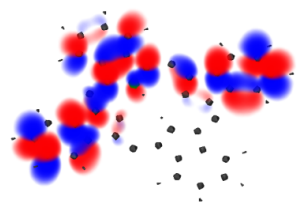
100



101

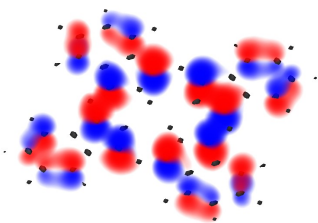


102

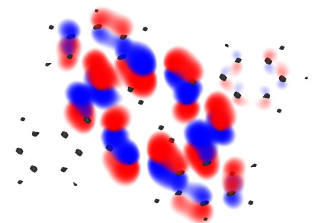


103

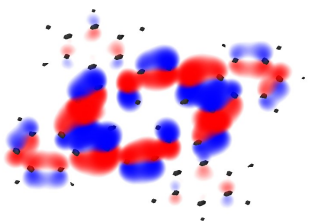
H₂ PC XAS TP calculation, N3 (green)



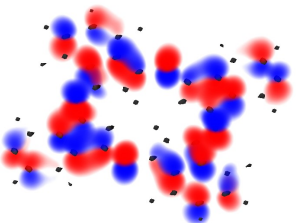
94 (HOMO)



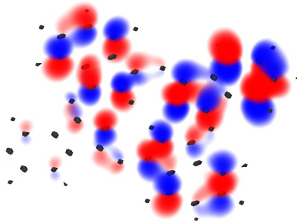
95 (LUMO)



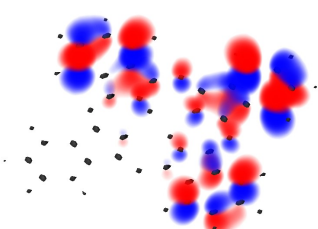
96



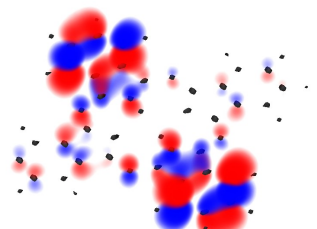
97



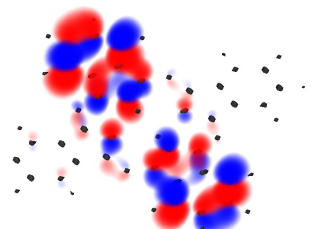
98



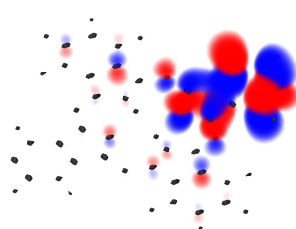
99



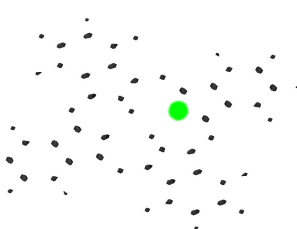
100



99-98

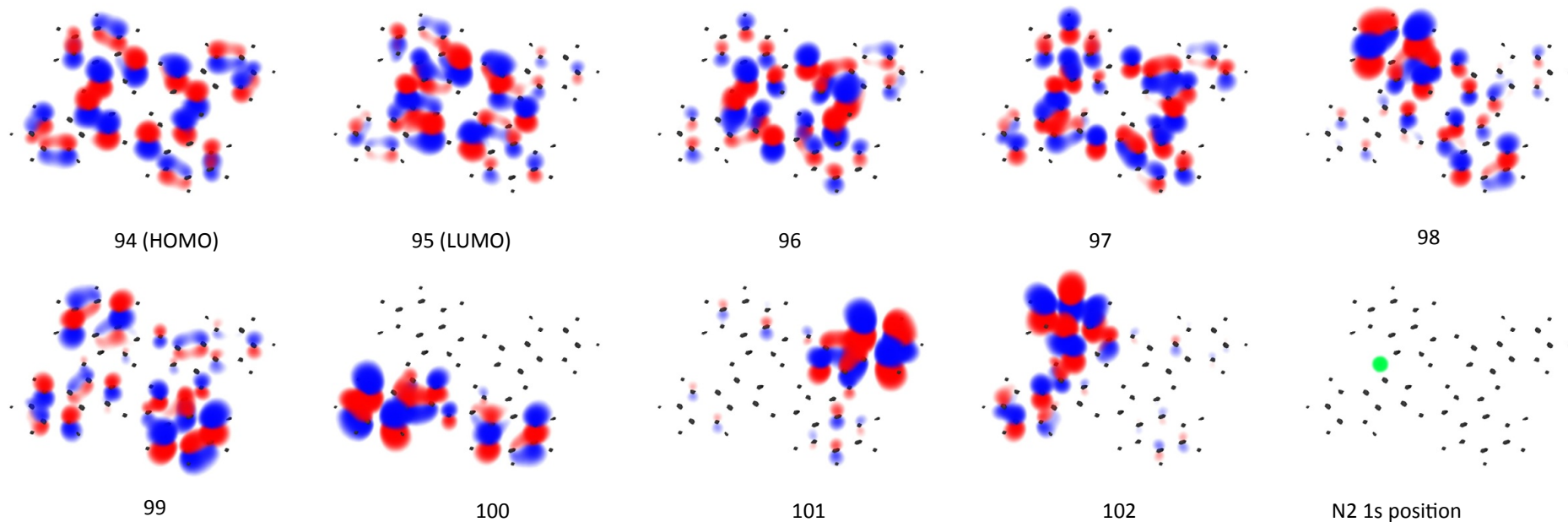


99+98

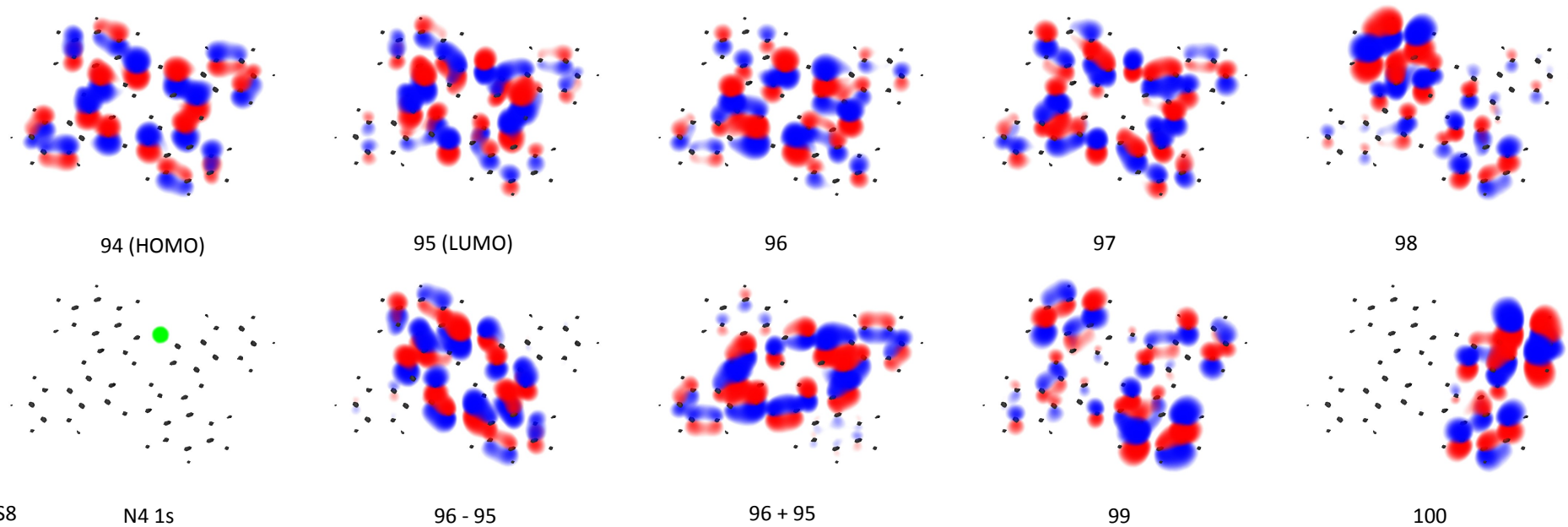


N3 1s

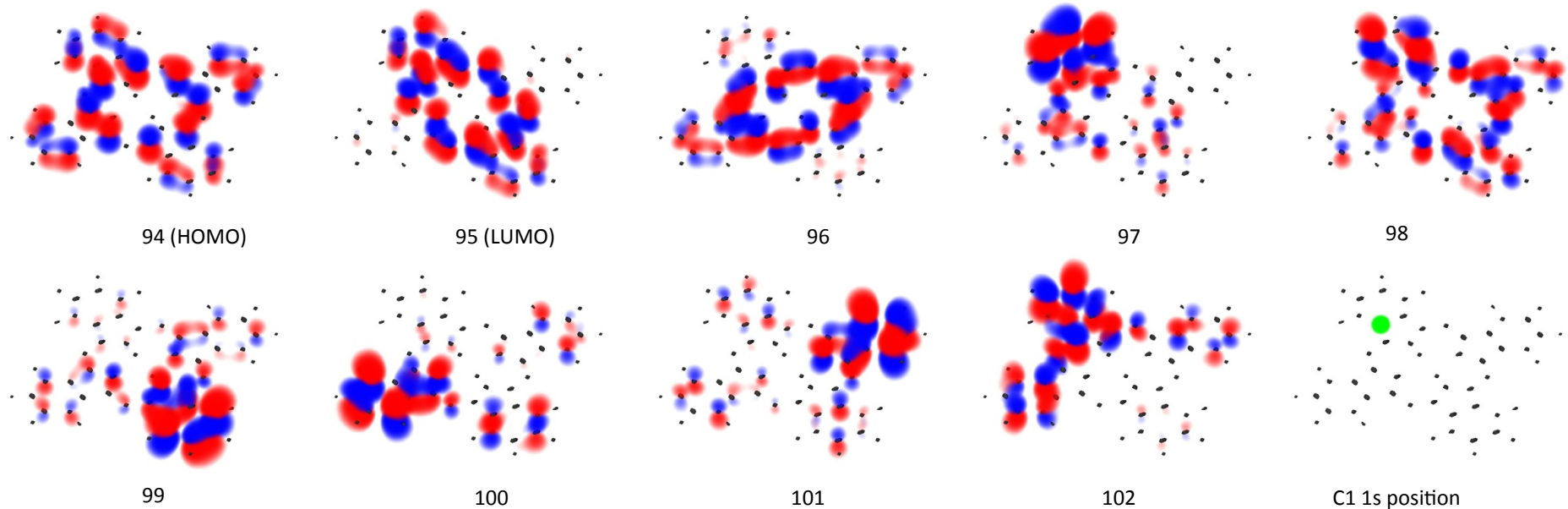
H₂ PC XAS TP Calculation, N2 (green)



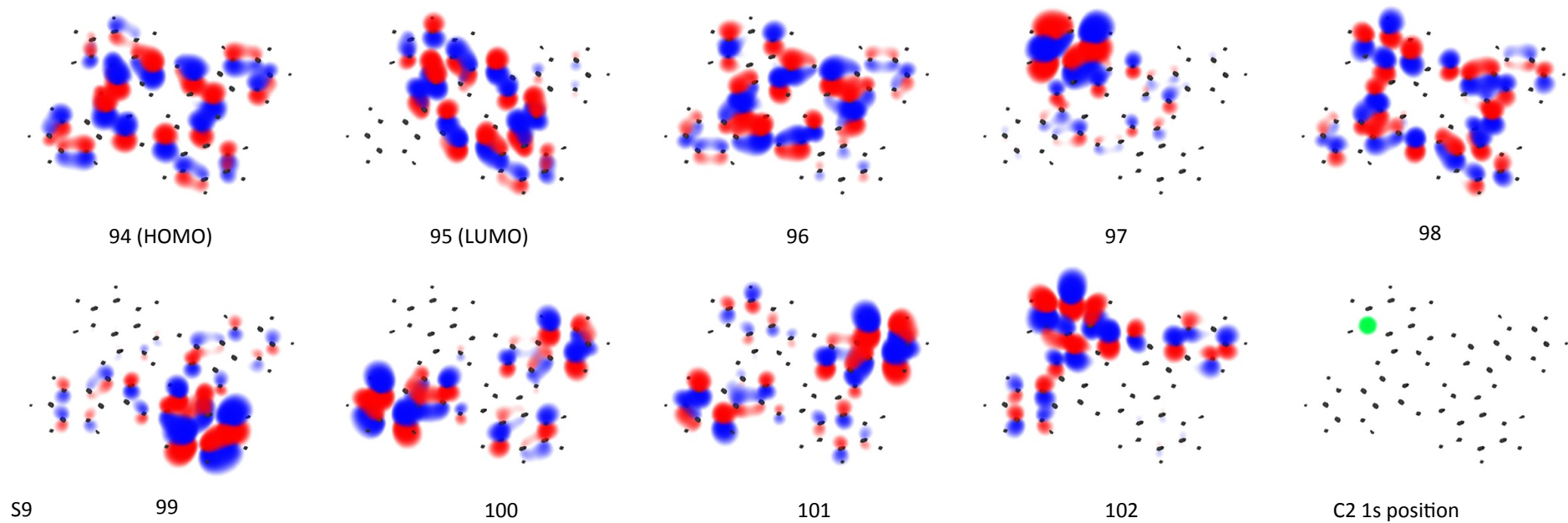
H₂ PC XAS TP Calculation, N4 (green)



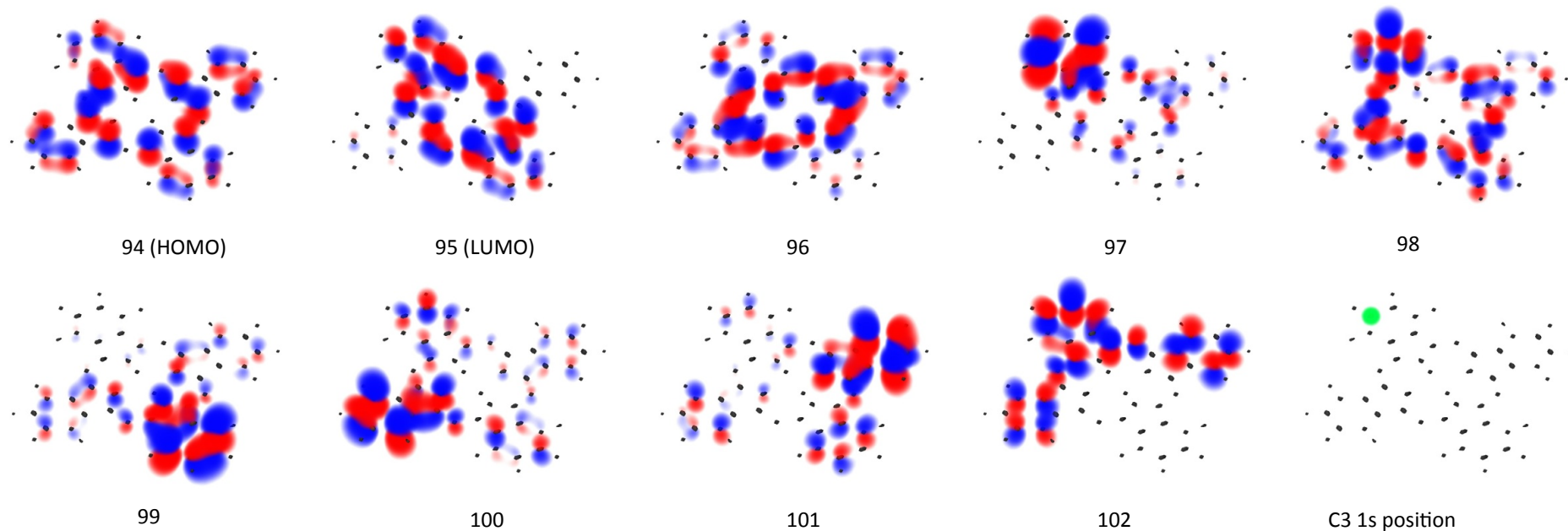
H₂ PC XAS TP Calculation, C1 (green)



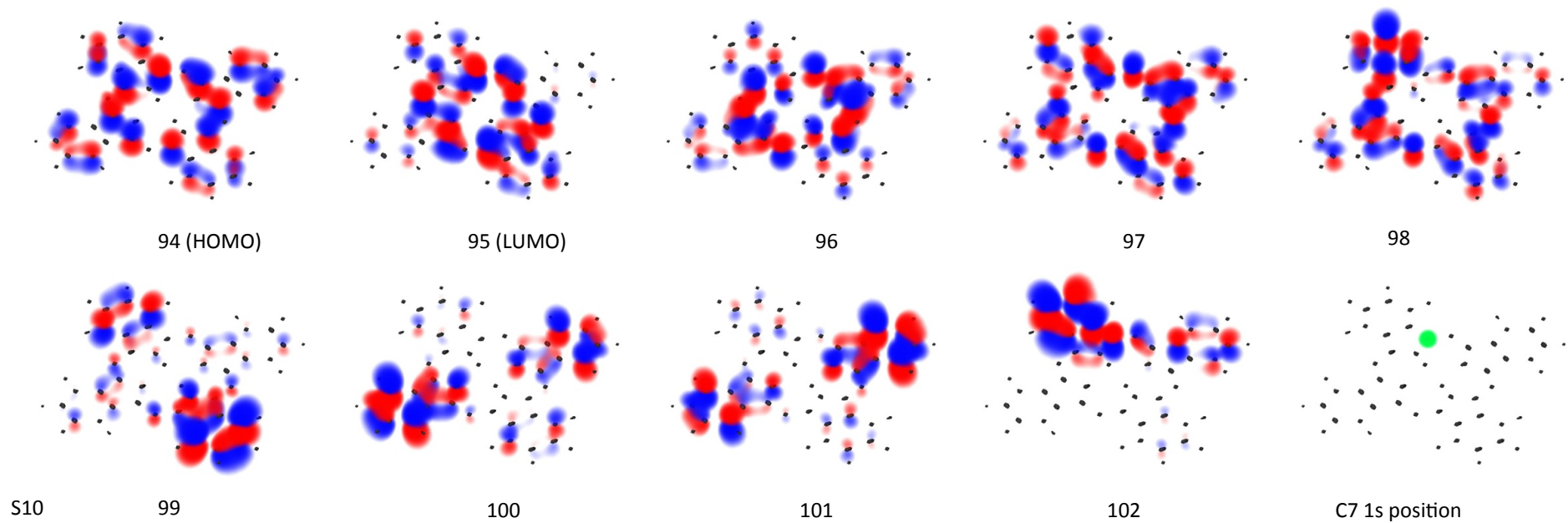
H₂ PC XAS TP Calculation, C2 (green)



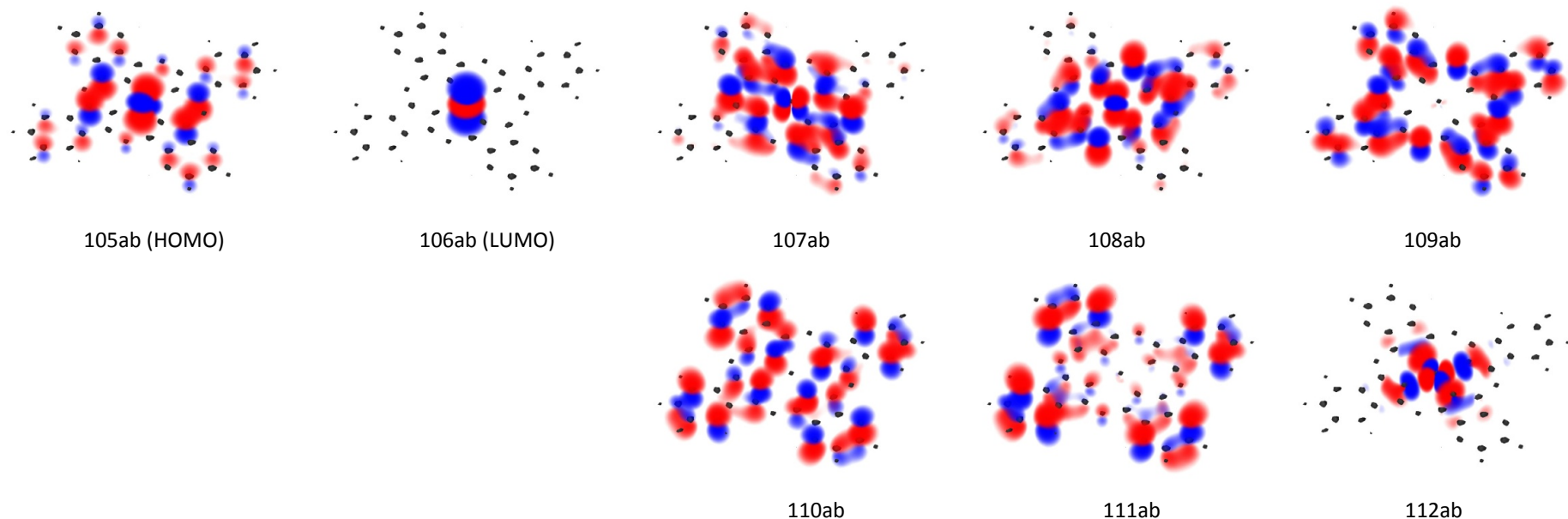
H₂ PC XAS TP Calculation, C3 (green)



H₂ PC XAS TP Calculation, C7 (green)

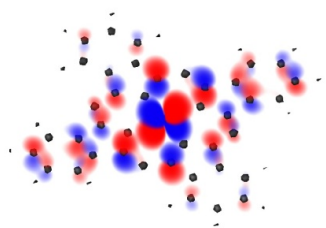


Fe PC Ground State Orbitals

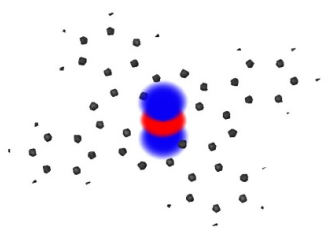


This page contains depictions of orbitals computed via StoBe for iron phthalocyanine. The LUMO is a d_z^2 state, the next two states are very similar to the H_2 phthalocyanine LUMOs, but with a high degree of d_{xz} and d_{yz} character at the metal center. One of the striking characteristics of these is that the d-orbitals seem somewhat rotated compared to what one might expect; the reason is unknown, but we posit either the rotation is real or a deficiency in the methods used for computation, and we make no further comment on its origin. The computations on the following page, used to obtain the XAS lineshape, are as expected with the d_{xz} and d_{yz} character around the metal center for the LUMO+1 states that otherwise resemble the H_2 phthalocyanine LUMOs. The b_{1g} orbital with $d_{x^2-y^2}$ character is at the metal center; orbital 111 in the Fe TP calculation.

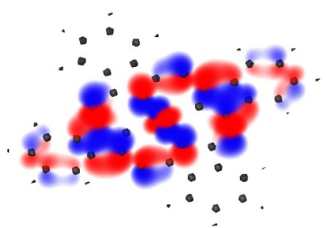
Fe PC Orbitals Fe TP Calculation



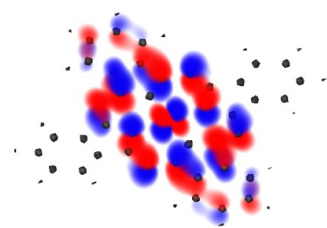
105a_HOMO



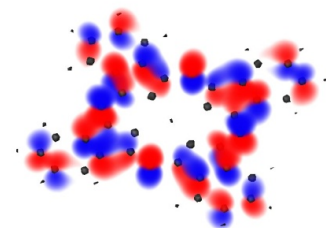
106a (LUMO)



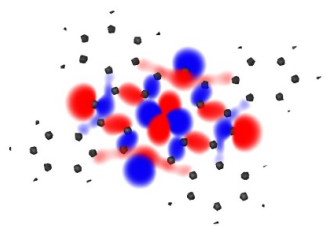
107ab



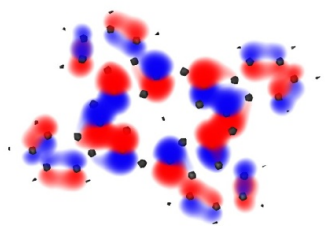
108ab



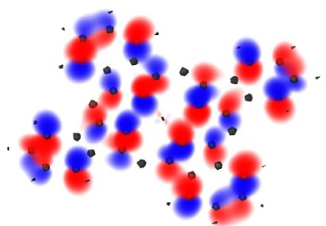
109ab



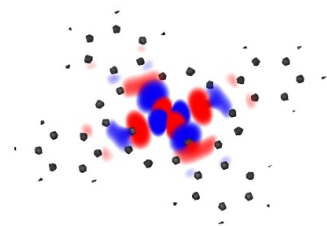
105b (HOMO)



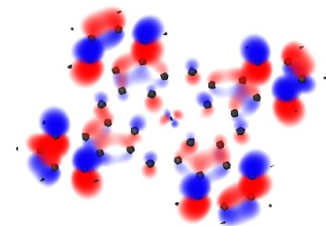
106b (LUMO)



110ab

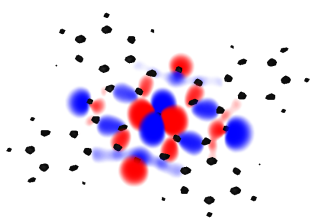


111ab

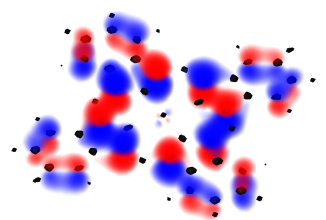


112ab

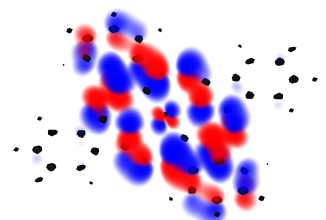
Fe PC N1 TP Orbitals



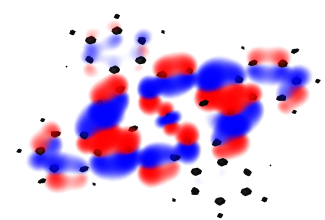
106a (HOMO)



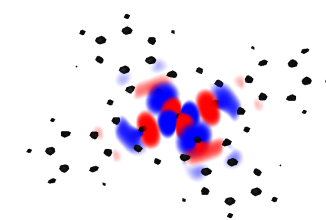
107a (LUMO)



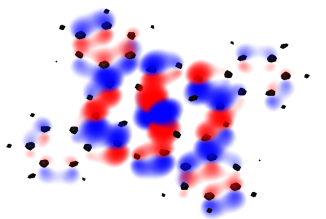
108a



109a

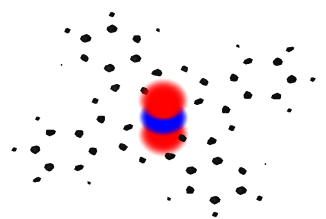


110a

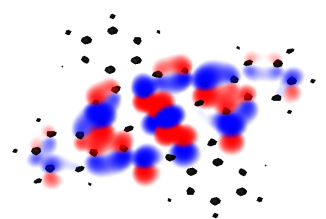


S12

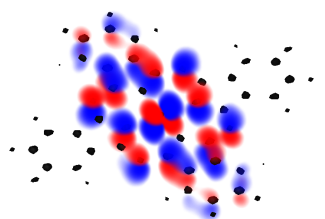
106b (HOMO)



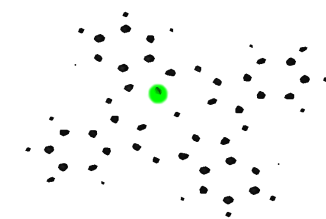
107b (LUMO)



108b

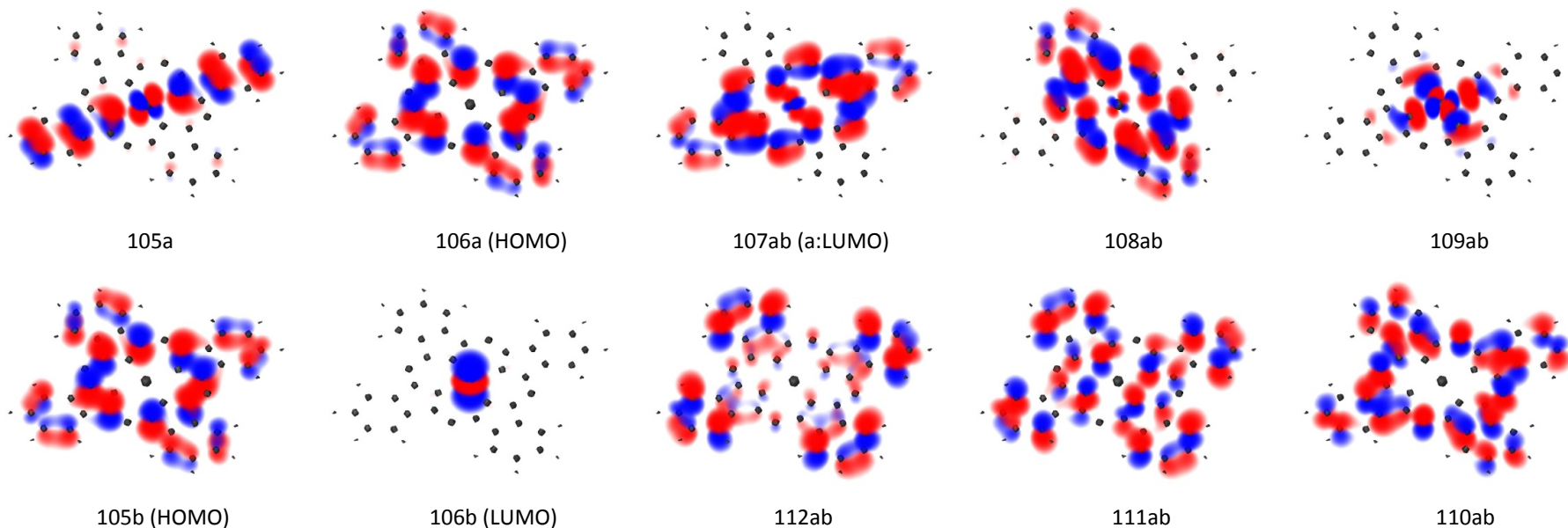


109b

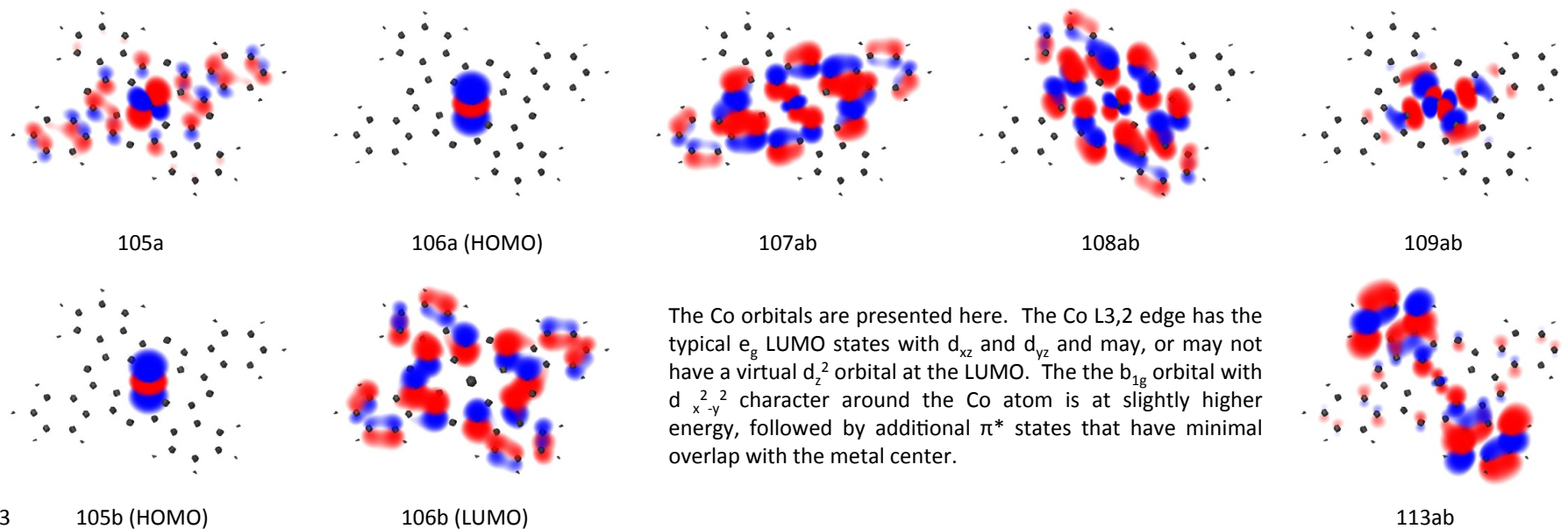


N1 1s

Co PC GS Orbitals

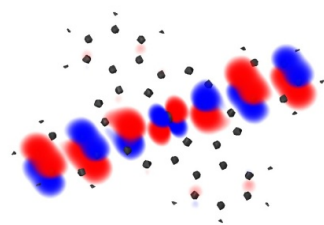


Co XAS TP Orbitals

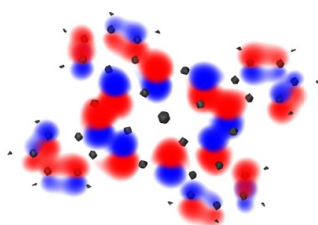


The Co orbitals are presented here. The Co L3,2 edge has the typical e_g LUMO states with d_{xz} and d_{yz} and may, or may not have a virtual d_{z^2} orbital at the LUMO. The b_{1g} orbital with $d_{x^2-y^2}$ character around the Co atom is at slightly higher energy, followed by additional π^* states that have minimal overlap with the metal center.

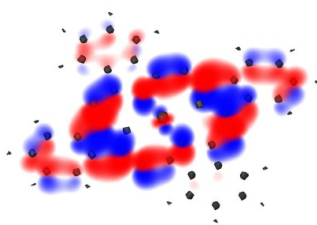
Co PC N1 TP XAS



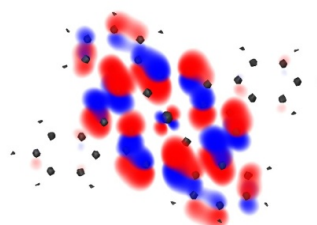
106a



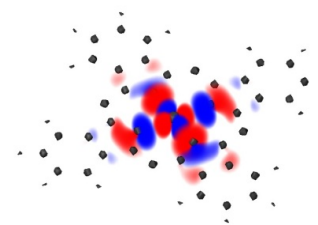
107a (HOMO)



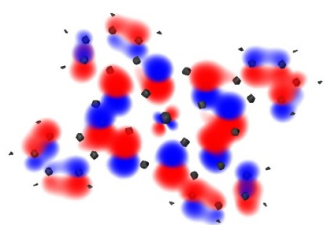
108ab (a:LUMO)



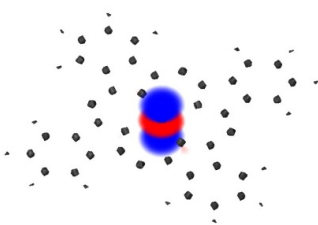
109ab



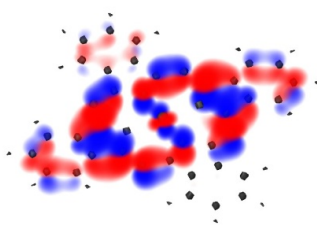
110ab



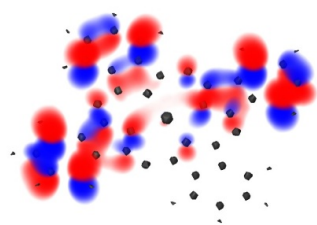
106b (HOMO)



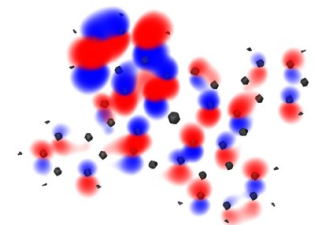
107b (LUMO)



108b

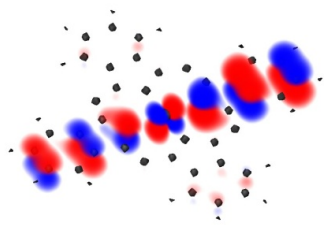


113ab

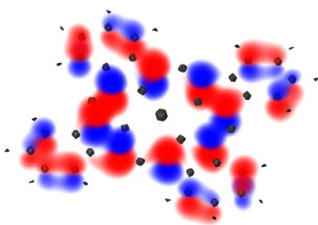


111ab

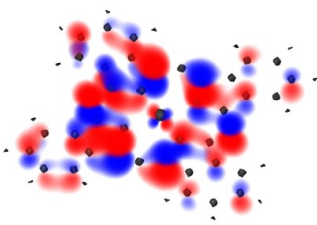
Co PC N2 TP XAS



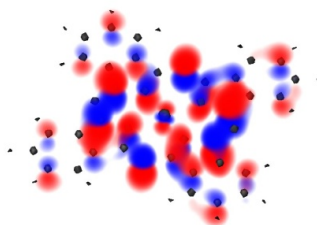
106a



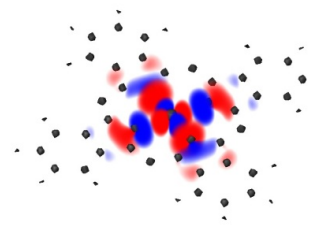
107a (HOMO)



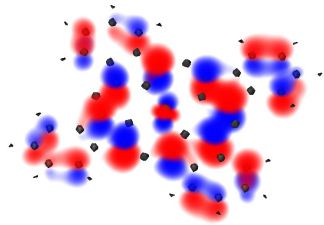
108a LUMO



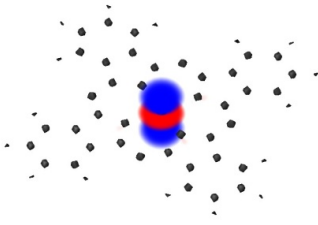
109ab



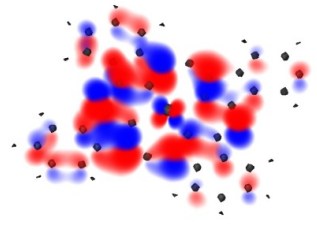
110ab



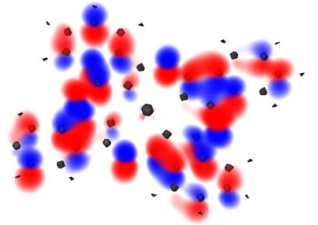
106b (HOMO)



107b (LUMO)



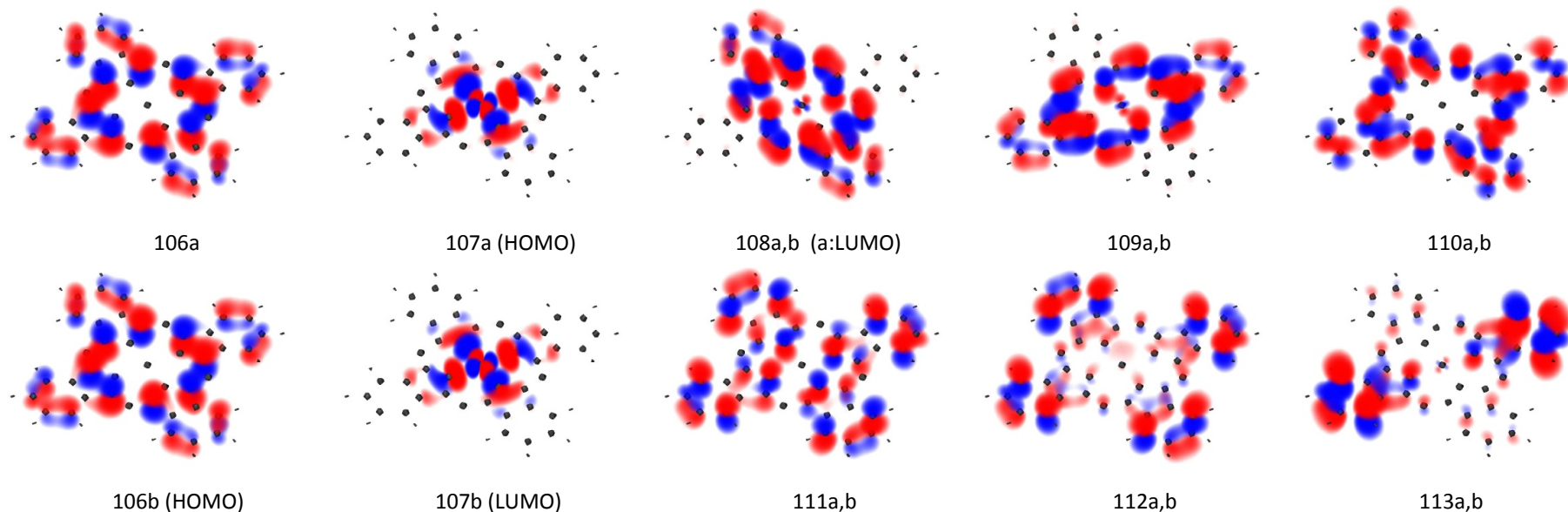
107b



111ab

Orbitals generated from TP calculations to generate Nitrogen XAS generally resemble H₂ phthalocyanine, with the exception of the orbital b_{1g} (orbital 110 ab) that, from the nitrogen prospective, has strong σ character.

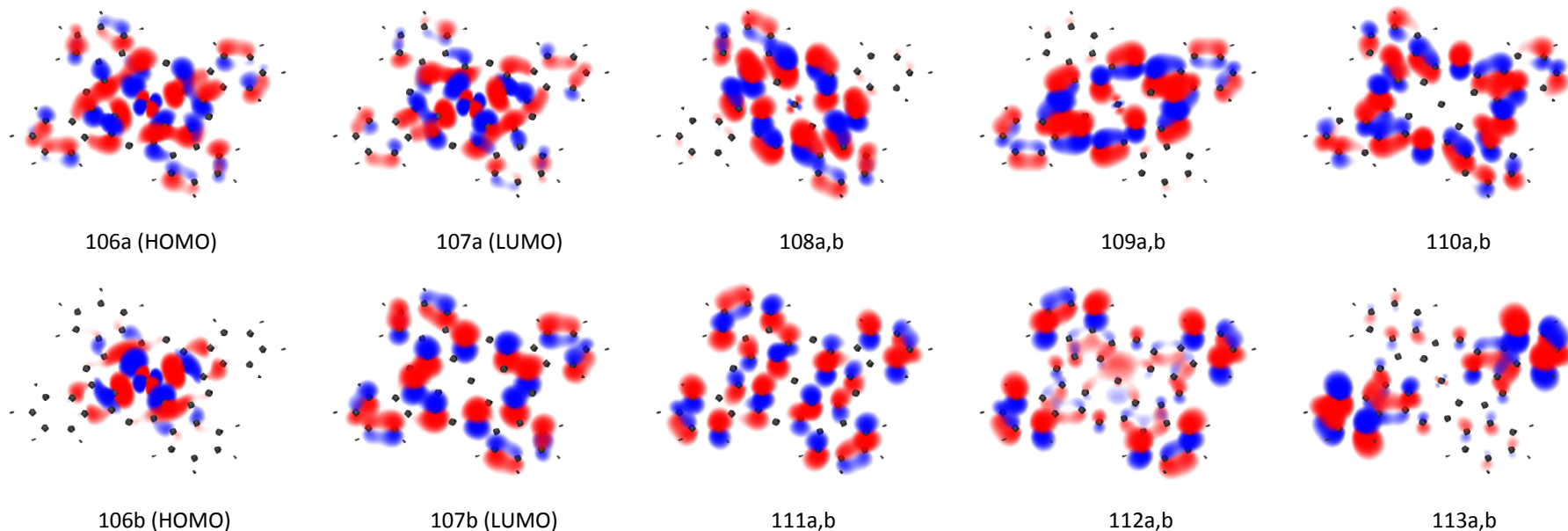
Cu Ground State Orbitals



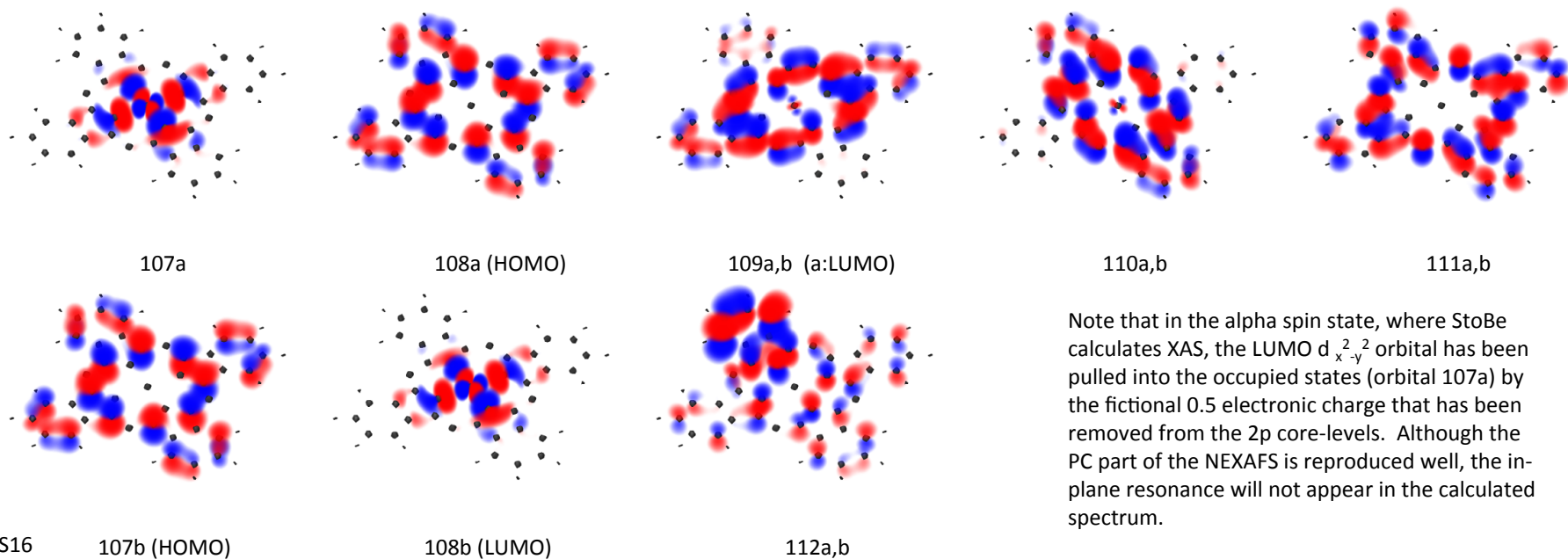
Copper orbitals represent an interesting case where the computation illustrates what is observed experimentally, but the level of theory we are using is not sufficient to reproduce the experiment without changing several input parameters. It is well-established that a SOMO (singly occupied molecular orbital) with $d_{x^2-y^2}$ character at the Cu central atom sits at the top of the HOMO / bottom of the LUMO (orbitals 107 a & b). Beyond this, the e_g and other π^* are similar to the orbitals found in H_2 phthalocyanine. In order to reproduce the NEXAFS spectrum, several computations with varying occupations at the core-level and varying overall charge were attempted to reproduce the spectra. We initially tried $\frac{1}{2}$ of a charge in the 2p states, and modified StoBe to ensure in the computation that the x-ray absorption was computed explicitly from the 3 different 2p states (StoBe orbitals 3, 4, and 5.) The x-rayspec appears to calculate the x-ray absorption in the alpha spin-state only, missing this LUMO. We tried unsuccessfully to explicitly to put the SOMO electron in a beta spin state to leave the alpha LUMO. Finally, removing 1 electron from the entire system (1 electron of the 293 (or 213 when pseudopotentials are used) keeps the LUMO $d_{x^2-y^2}$ orbital virtual, and reproduces the experimental spectrum remarkably well. The same is true for nitrogen: the peak running counter to the π^* was apparent when both 1 electron is completely removed, and a core-level charge of 0.3 was removed from the 2p Cu states for the TP computation. Orbitals from these TP calculations appear on the next few pages.

Cu PC XAS TP calc. for Cu, 0.5 2p core, ion

Note that 106a + 106b gives something that looks like gs 107b, and 106a-107a gives gs 106a. These parameters reproduced the experimental Cu $L_{3,2}$ NEXAFS relatively well.

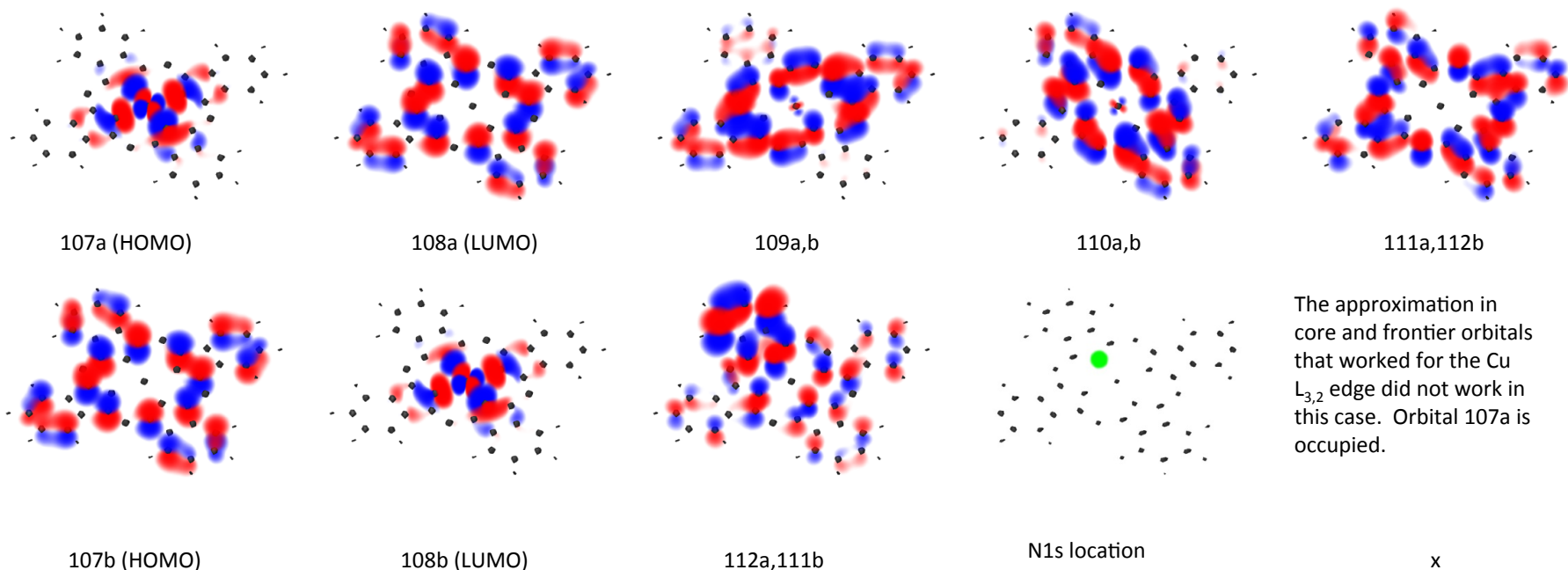


Cu PC TP calc. for N1, 0.5 core-hole.



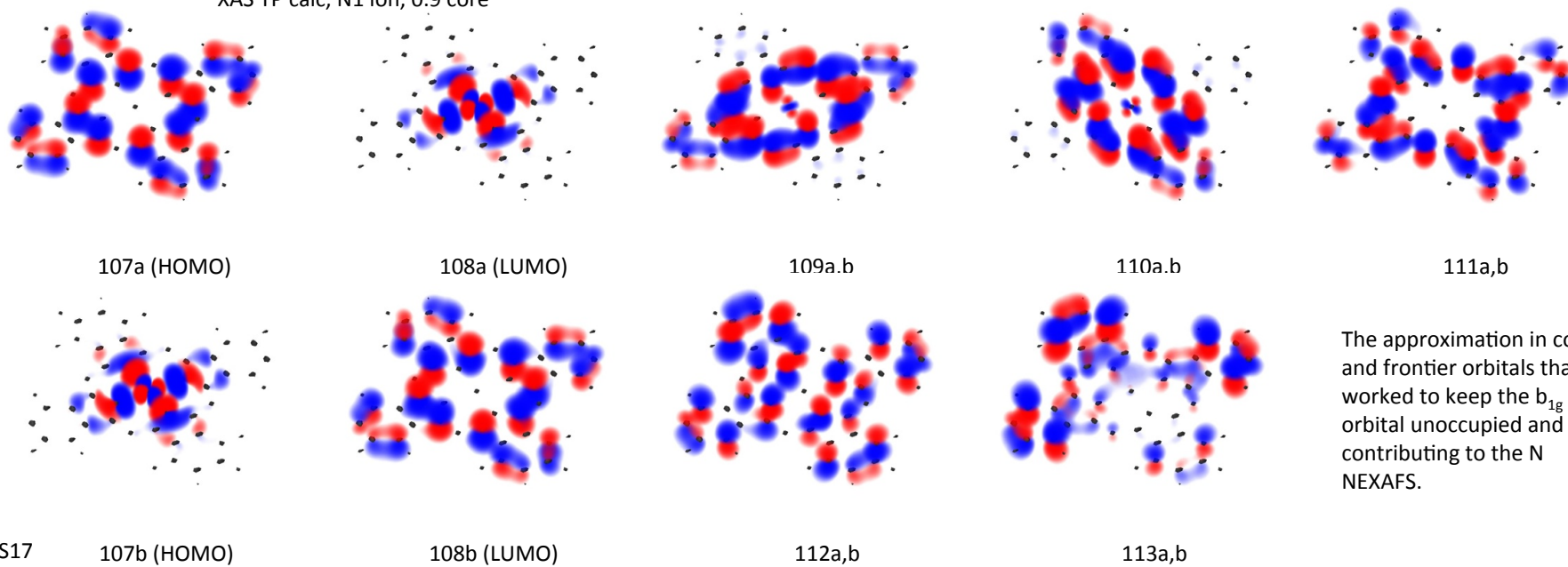
Note that in the alpha spin state, where StoBe calculates XAS, the LUMO $d_{x^2-y^2}$ orbital has been pulled into the occupied states (orbital 107a) by the fictional 0.5 electronic charge that has been removed from the 2p core-levels. Although the PC part of the NEXAFS is reproduced well, the in-plane resonance will not appear in the calculated spectrum.

Cu PC TP calc., N1, 0.5 electron in the N 1s, 1 additional electron removed



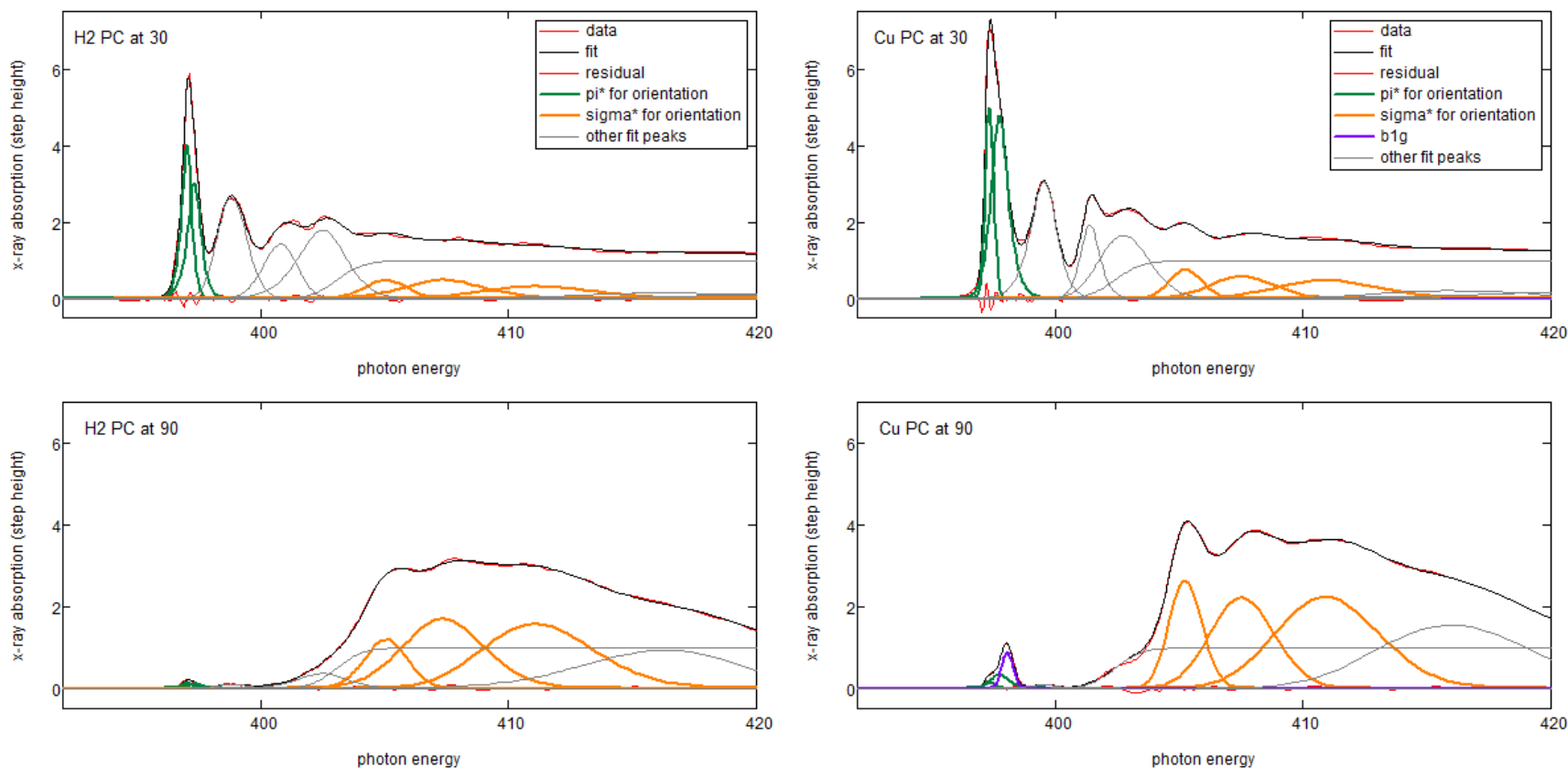
The approximation in core and frontier orbitals that worked for the Cu $L_{3,2}$ edge did not work in this case. Orbital 107a is occupied.

XAS TP calc, N1 ion, 0.9 core



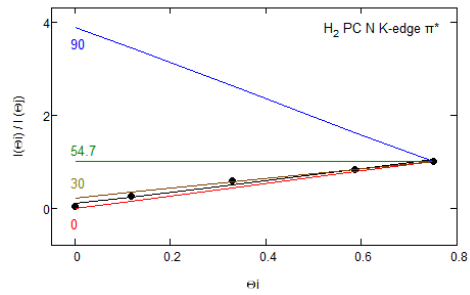
The approximation in core and frontier orbitals that worked to keep the b_{1g} orbital unoccupied and contributing to the N NEXAFS.

Peak fits for two representative phthalocyanines; N K-edge.

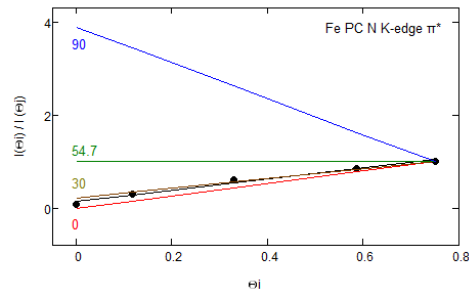


To determine orientations, each set N K-edge data were fit using a custom-written code with the fewest possible peaks to get a reasonable fit. In the panes above, the experimental data (red) is presented, along with this fit (black) and residual (red). The constituent peaks that make up the fit are also presented. The most intense, lowest energy π^* was used to determine orientation; this was best fit by a doublet, and these peaks are indicated in green. The three most prominent σ^* peaks, shown in orange, were also used for determining orientation. Finally, the b1g peak, due to N-Cu bonding, is presented in purple.

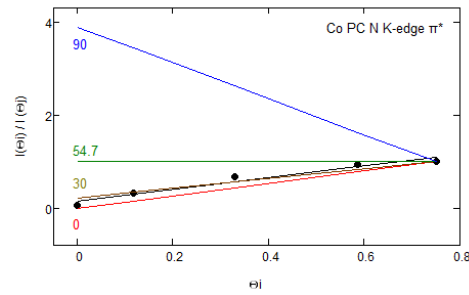
Intensity plots for π^* and σ^* resonances, as outlined in the previous slide for the N K-edges.



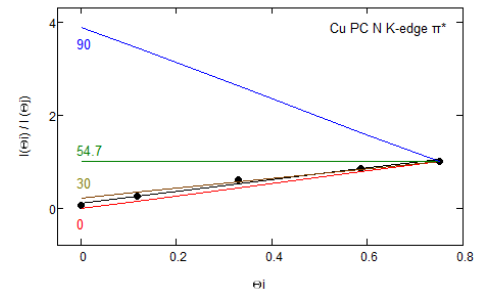
15.7 degrees
high: 23.4 degrees
low: <0 degrees



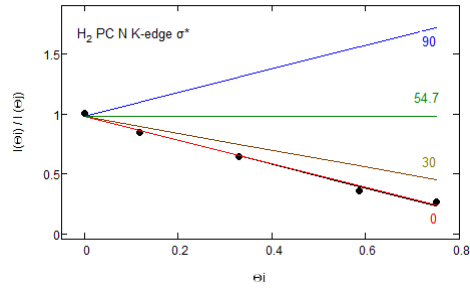
21.7 degrees
high: 27.4 degrees
low: 13.0 degrees



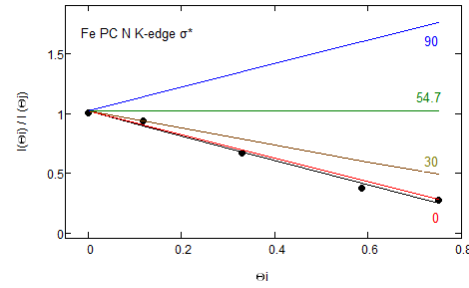
16.5 degrees
high: 27.6 degrees
low: <0 degrees



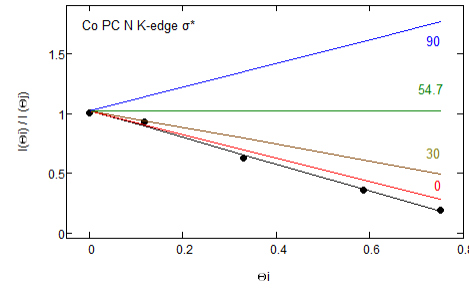
16.8 degrees
high: 24.5 degrees
low: <0 degrees



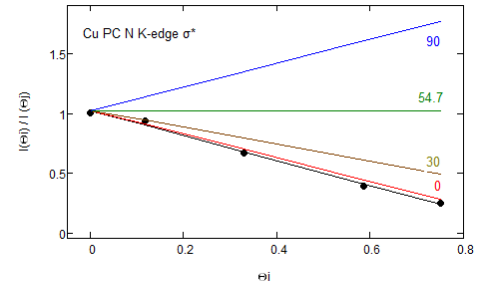
0 degrees
high: 12.1 degrees
low: <0 degrees



0 degrees
high: 7.7 degrees
low: <0 degrees



0 degrees
high: <0 degrees
low: <0 degrees



0 degrees
high: <0 degrees
low: <0 degrees

The intense white-line resonance in the Cu L-edges, as an in-plane resonance also supports 0 degrees for Cu-PC.

